nature microbiology

Article

https://doi.org/10.1038/s41564-024-01901-9

Shigella infection is facilitated by interaction of human enteric α-defensin 5 with colonic epithelial receptor P2Y11

Received: 28 February 2024

Accepted: 2 December 2024

Dan Xu[1,8], **Mengyao Guo**[1,8], **Xin Xu**[1], **Gan Luo**[2], **Yaxin Liu**[1], **Stephen J. Bush**[3], **Chengyao Wang**[4], **Tun Xu**[3], **Wenxin Zeng**[1], **Chongbing Liao**[2], **Qingxia Wang**[2], **Wei Zhao**[4], **Wenying Zhao**[1], **Yuezhuangnan Liu**[1], **Shanshan Li**[1], **Shuangshuang Zhao**[5], **Yaming Jiu**[5], **Nathalie Sauvonnet**[6,9], **Wuyuan Lu**[2,9] ✉, **Philippe J. Sansonetti**[5,7,9] ✉ & **Kai Ye**[1,3,4,9] ✉

Human enteric α-defensin 5 (HD5) is an immune system peptide that acts as an important antimicrobial factor but is also known to promote pathogen infections by enhancing adhesion of the pathogens. The mechanistic basis of these conflicting functions is unknown. Here we show that HD5 induces abundant filopodial extensions in epithelial cells that capture *Shigella*, a major human enteroinvasive pathogen that is able to exploit these filopodia for invasion, revealing a mechanism for HD5-augmented bacterial invasion. Using multi-omics screening and in vitro, organoid, dynamic gut-on-chip and in vivo models, we identify the HD5 receptor as P2Y11, a purinergic receptor distributed apically on the luminal surface of the human colonic epithelium. Inhibitor screening identified cAMP-PKA signalling as the main pathway mediating the cytoskeleton-regulating activity of HD5. In illuminating this mechanism of *Shigella* invasion, our findings raise the possibility of alternative intervention strategies against HD5-augmented infections.

Human enteric α-defensin 5 (HD5), an abundant immunoprotective peptide produced by Paneth cells of the small intestine[1–4], can, surprisingly, promote the infection of pathogens including *Shigella* and human immunodeficiency virus (HIV)[5–10]. However, the molecular basis of this is poorly understood, not only because of the unique properties of the pathogens involved but the promiscuous binding behaviour of HD5, which, to the best of our knowledge, still lacks a bona fide receptor for a specific cellular function.

Exploiting filopodial extensions is a common invasion strategy for pathogens that establish intimate contact with host cells either by associating with pre-existing filopodia or inducing additional filopodia to enable more efficient infection[11–14]. *Shigella* is a prominent example since its capture by filopodia-like structures is the principal means by which it makes initial contact with host cells, given its intrinsic lack of adhesin and invasin[15–17]. Nonetheless, *Shigella*'s entry into host cells in in vitro models is surprisingly inefficient as spontaneous filopodia are

---

[1]Key Laboratory of Biomedical Information Engineering (MOE), School of Life Science and Technology, Xi'an Jiaotong University, Xi'an, China. [2]Key Laboratory of Medical Molecular Virology (MOE/NHC/CAMS), School of Basic Medical Science, Fudan University, Shanghai, China. [3]School of Automation Science and Engineering, Faculty of Electronic and Information Engineering, Xi'an Jiaotong University, Xi'an, China. [4]The First Affiliated Hospital, Xi'an Jiaotong University School of Medicine, Xi'an, China. [5]CAS Key Laboratory of Molecular Virology and Immunology, Shanghai Institute of Immunity and Infection, Chinese Academy of Sciences, Shanghai, China. [6]Tissue Homeostasis group, Biomaterials and Microfluidics Core Facility, Institut Pasteur, Université Paris Cité, Paris, France. [7]Institut Pasteur, Paris, France. [8]These authors contributed equally: Dan Xu, Mengyao Guo. [9]These authors jointly supervised this work: Nathalie Sauvonnet, Wuyuan Lu, Philippe J. Sansonetti, Kai Ye. ✉e-mail: luwuyuan@fudan.edu.cn; philippe.sansonetti@pasteur.fr; kaiye@xjtu.edu.cn

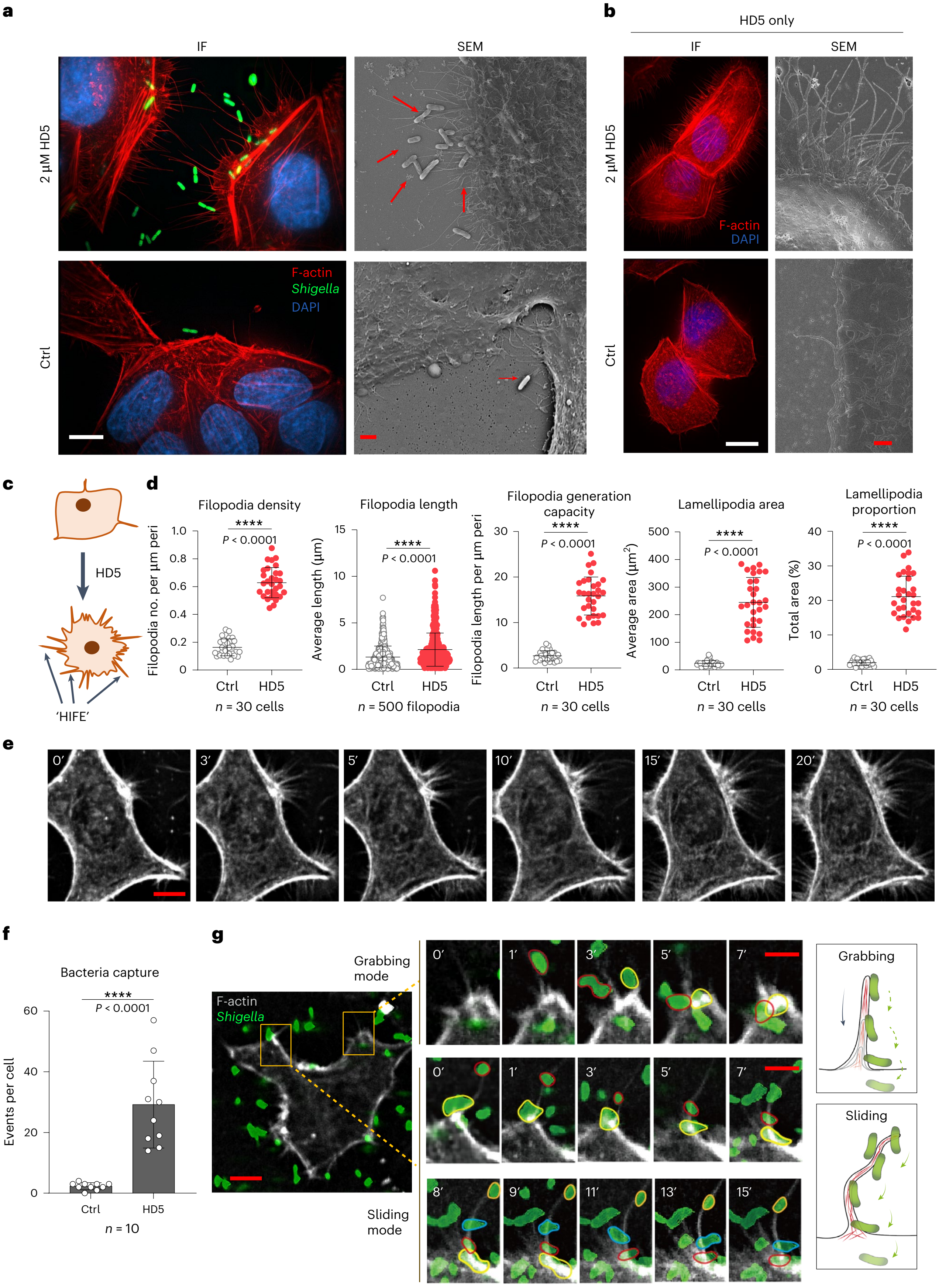
a
IF
SEM
2 µM HD5
Ctrl
F-actin
Shigella
DAPI
b
HD5 only
IF
SEM
2 µM HD5
Ctrl
F-actin
DAPI
c
HD5
'HIFE'
d
Filopodia density
Filopodia no. per µm peri
****
P < 0.0001
Ctrl
HD5
n = 30 cells
Filopodia length
Average length (µm)
****
P < 0.0001
n = 500 filopodia
Filopodia generation capacity
Filopodia length per µm peri
****
P < 0.0001
n = 30 cells
Lamellipodia area
Average area (µm²)
****
P < 0.0001
n = 30 cells
Lamellipodia proportion
Total area (%)
****
P < 0.0001
n = 30 cells
e
0′
3′
5′
10′
15′
20′
f
Bacteria capture
Events per cell
****
P < 0.0001
Ctrl
HD5
n = 10
g
Grabbing mode
Sliding mode
F-actin
Shigella
0′
1′
3′
5′
7′
8′
9′
11′
13′
15′
Grabbing
Sliding

Fig. 1 | HD5 induces rapid formation of filopodia that capture *Shigella* in the early stage of infection. **a**, Fluorescence microscopy (IF, left) and scanning electron microscopy (SEM, right) analysis of interaction between *Shigella* Sf301 strain and HeLa cells after 10 min in the absence (control) or presence of 2 µM HD5 (MOI = 50). GFP-expressing bacteria are green, F-actin is red and nuclei are blue (DAPI). Scale bar, 10 µm (IF images), 3 µm (SEM images). Red arrows, bacteria. **b**, IF (left) and SEM (right) analysis of cytoskeleton of HeLa cells in the absence (control) or presence of 2 µM HD5. F-actin is red and nuclei are blue (DAPI). Scale bar, 10 µm (IF images), 3 µm (SEM images). **c**,**d**, Schematic illustration (**c**) and quantitative characterization (**d**) of 'HD5-induced filopodial extensions (HIFE)'. Density, average length, generation capacity of filopodia, actual and relative area of lamellipodia stimulated by 2 µM HD5 were measured uaing Filoquant and ImageJ as described in Methods ($n = 30$). Data are mean ± s.d. **e**, Time-sequential acquisition of real-time actin alteration induced by HD5 in SiR-actin-labelled live HeLa cells. F-actin is grey. Scale bar, 10 µm. **f**, Quantitative characterization of bacterial capture events from 10 randomly-selected cells of time-lapse fluorescence microscopy ($n = 10$). Data are mean ± s.d. **g**, Time-sequential acquisition of real-time *Shigella* capture by filopodia extensions induced by HD5 in SiR-actin-labelled HeLa. F-actin is grey and bacteria are green. Individual *Shigella* was outlined with red, yellow, orange or cyan colour, which respectively represents independent moving bacterium in the dynamic images. Scale bar, 10 µm (whole view), 5 µm (inset views). Right: schematic illustration of the grabbing and sliding patterns of bacterial motion towards the cell body. Significance was determined using two-tailed unpaired Student's *t*-test (**d**,**f**); $^{****}P < 0.0001$.

sparse and fragile, which, in addition to the fact that *Shigella* does not adhere strongly to cells, results in a low efficiency of bacterial capture and invasion that can hardly justify its high infectivity in vivo[16,17].

Here we show that HD5 by itself induces abundant filopodial extensions in human epithelial cells, which *Shigella* exploits to enhance contact with host cells (importantly, invasion of colonic epithelial cells is the critical first step in *Shigella* pathogenesis[18,19]). We further demonstrate that human purinergic receptor P2Y11 is both the main receptor responsible for interacting with HD5 and the mediator for cytoskeletal reorganization via the cAMP-protein kinase A (PKA) pathway. To the best of our knowledge, this is the HD5 receptor that has never been reported before to be associated with a specific cellular function, of note because P2Y11 intervention was demonstrably effective in attenuating HD5-mediated *Shigella* invasion in in vitro, in vivo, organoid and dynamic gut-on-chip models.

Results

HD5 induces filopodia to capture *Shigella* in early infection

To investigate the detailed mechanisms of the infection-promoting activity of HD5, in vitro *Shigella* infection assays were performed on HeLa cells in the presence of HD5 at physiological concentrations[5,6]. Immunofluorescence (IF) and scanning electron microscopy (SEM) analysis indicated that HeLa cells underwent substantial cytoskeletal rearrangements within 15 min in the presence of both 2 µM HD5 and *Shigella*, characterized by large-scale formation of filopodial extensions, which over 90% of the observed *Shigella* were associated with (Fig. 1a).

We next found that HD5 alone, at 0.5 to 4 µM, induced rapid rearrangements of the cytoskeleton, reaching saturation at 2 µM within 15 min (Fig. 1b and Extended Data Fig. 1a). We name these 'HD5-induced filopodial extensions' (HIFE) (Fig. 1c). By contrast, *Shigella* alone, even at a high multiplicity of infection (MOI) of 100, did not result in comparable cytoskeletal changes within the same time frame (Extended Data Fig. 1b).

To gain insight into the morphodynamic characteristics of HIFE, we used FiloQuant[20] and found that upon HD5 stimulation, the average length and density of filopodia increased by 1.5 and 3.8-fold, respectively (Fig. 1d). We then combined these two parameters to define the filopodia generation capacity (FGC) which HD5 increased by 5.9-fold. Using ImageJ[21], we also found that both the actual and relative area of lamellipodia increased over 10-fold in HD5-stimulated cells (Fig. 1d). More importantly, dynamic analysis revealed that filopodia reached their maximum length of 8–12 µm within 10 min, followed by retraction to the cell body while more waves succeeded (Fig. 1e and Supplementary Video 1).

Dynamic capturing of *Shigella* by HIFE was observed using SiR-actin-labelled live HeLa cells and GFP-expressing *Shigella*. In mock-treated cells, 2.3 ± 1.5 spontaneous capture events per cell were observed within 30 min, while HD5 increased these capture events to 29.2 ± 17.8 per cell (Fig. 1f, and Supplementary Videos 2 and 3). Stepwise observation revealed that following the initial contact by HIFE, two distinct modes of bacterial motion towards the cell body could be identified (Fig. 1g). Of 153 observed HIFE-associated bacteria, 146 were 'grabbed' to the cell body when the filopodium retracted at a speed of 3.1 ± 1.7 µm min^{-1}. In contrast, the remaining 5% of HIFE-associated bacteria were found to 'slide' along the filopodium to the cell body instead, at a lower speed of 1.2 ± 0.7 µm min^{-1} (Fig. 1g).

HIFE capture boosts invasion efficiency of *Shigella*

To validate a causal link between HIFE and *Shigella* invasion, *Shigella* Sf301 was allowed to adhere onto HeLa cells by 10-min centrifugation, followed by thorough washing to remove non-adhering bacteria (Fig. 2a). While the spontaneous invasion of already-adhering *Shigella* occurred at low efficiency (2%) within 30 min, 2 µM HD5 increased the invasion efficiency of already-adhering Sf301 to 36% (Fig. 2b). Furthermore, HD5 was allowed to interact with *Shigella* or HeLa cells separately for 15 min and then removed (Extended Data Fig. 1c). HD5-coated *Shigella*, which exhibited much higher adhesiveness than mock-treated Sf301 (26% vs 5% of input), invaded HeLa cells at a relatively low efficiency of 4% (Fig. 2c). However, when HD5-coated *Shigella* infected HD5-primed HeLa cells, invasion was substantially increased compared with mock-treated cells (107% vs 4%) despite no significant

Fig. 2 | HIFE capture boosts invasion efficiency of *Shigella*. **a**, Experimental procedure to examine the role of HD5 on *Shigella* invasion. **b**, Effects of 2 µM HD5 on Sf301 invasion when added after the adhesion step. Adhesion is defined as the total number c.f.u.s of HeLa cell-associated bacteria after 10-min centrifugation. Left: invasion is expressed as the c.f.u.s of intracellular bacteria in HeLa cells in the subsequent 30 min. Right: invasion efficiency is presented as the percentage of invasion/adhesion ($n = 6$). Data are mean ± s.d. **c**, HD5 was allowed to interact with *Shigella* (HD5-bound Sf301) or HeLa cell (HD5-primed HD5) separately for 15 min, followed by 3 thorough washes, and adhesion and invasion assays were performed with different combinations as indicated ($n = 6$). Data are mean ± s.d. Right: fluorescence microscopy examination of bacteria–cell interactions in all combinations after 30 min of infection. GFP-expressing bacteria are green, F-actin is red and nuclei are blue (DAPI). White arrows, actin foci (indicator of active *Shigella* invasion). Scale bar, 20 µm. **d**, Graphic illustration of the two distinct roles of HD5 in *Shigella* infection by acting on bacteria and on host cell, respectively. **e**, The influence of 10 µM cytochalasin D on *Shigella* adhesion and invasion in the presence and absence of 4 µM HD5. Top: GFP-expressing bacteria are green, F-actin is red and nuclei are blue (DAPI). Scale bar, 20 µm. Bottom: data are mean ± s.d ($n = 6$). **f**,**g**, Fluorescence emission spectra analysis (**f**) and fluorescence microscopic analysis (**g**) of CCF4-AM-loaded HeLa cells infected with Sf301 carrying a reporter gene of *bla* fused with *ipgD* in the different combinations described in **c** and Extended Data Fig. 1c. In **f**, data points are mean ± s.d. ($n = 3$). In **g**, scale bar represents 50 µm. Significance was determined using two-tailed unpaired Student's *t*-test (**b**,**e**) or one-way analysis of variance (ANOVA) (with Tukey's multiple comparisons test) (**c**); $^{**}P < 0.01$, $^{****}P < 0.0001$; NS, no significance. All results are representative of at least 3 independent experiments.

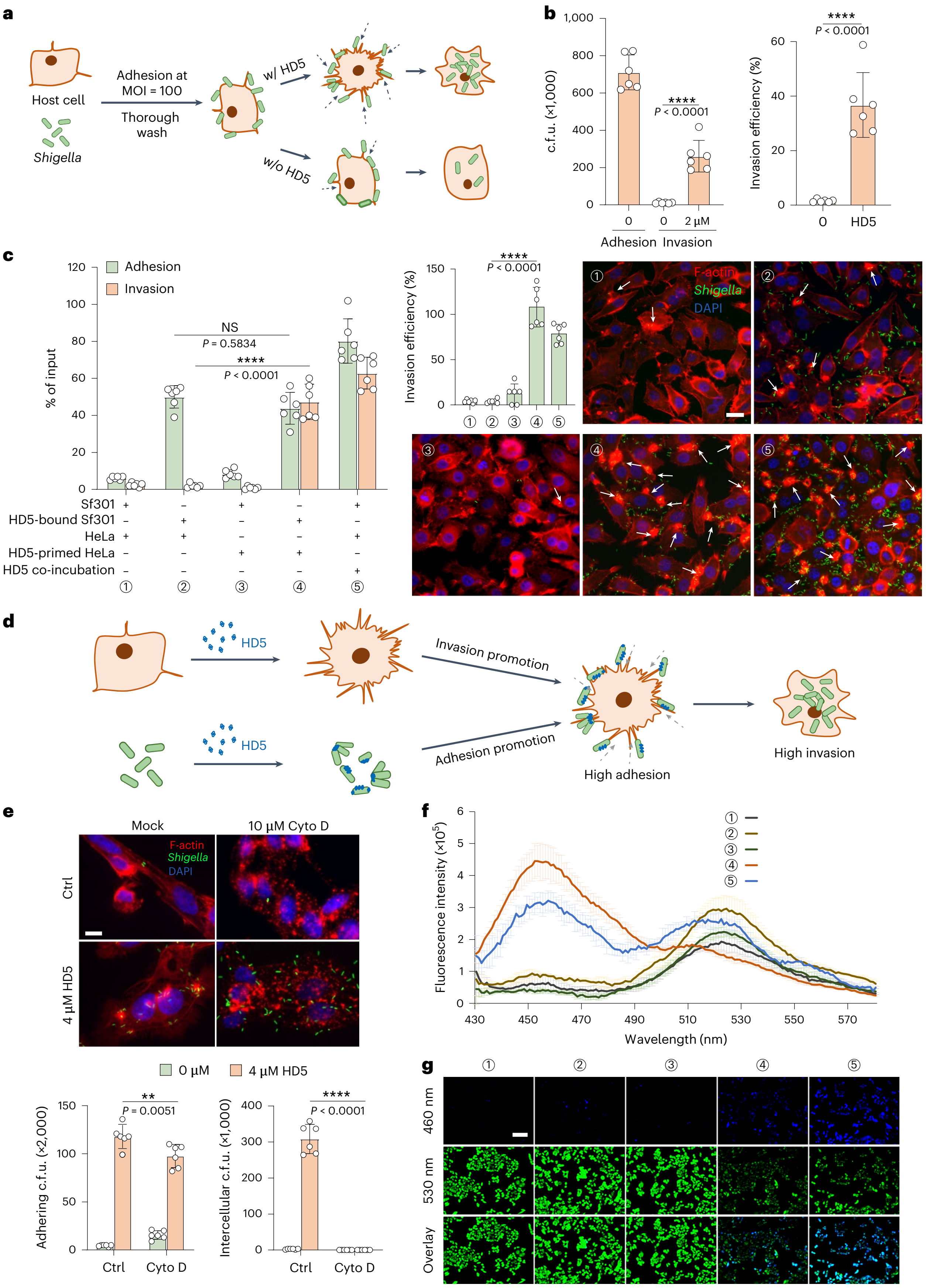
a
Host cell
Shigella
Adhesion at MOI = 100
Thorough wash
w/ HD5
w/o HD5
b
c.f.u. (×1,000)
1,000
800
600
400
200
0
****
P < 0.0001
0
0
2 µM
Adhesion
Invasion
Invasion efficiency (%)
60
40
20
0
****
P < 0.0001
0
HD5
c
Adhesion
Invasion
% of input
120
100
80
60
40
20
0
NS
P = 0.5834
****
P < 0.0001
Sf301 + − + − +
HD5-bound Sf301 − + − + −
HeLa + + − − +
HD5-primed HeLa − − + + −
HD5 co-incubation − − − − +
① ② ③ ④ ⑤
Invasion efficiency (%)
150
100
50
0
****
P < 0.0001
① ② ③ ④ ⑤
F-actin
Shigella
DAPI
d
HD5
HD5
Invasion promotion
Adhesion promotion
High adhesion
High invasion
e
Mock
10 µM Cyto D
Ctrl
4 µM HD5
F-actin
Shigella
DAPI
0 µM
4 µM HD5
Adhering c.f.u. (×2,000)
150
100
50
0
**
P = 0.0051
Ctrl
Cyto D
Intercellular c.f.u. (×1,000)
400
300
200
100
0
****
P < 0.0001
Ctrl
Cyto D
f
Fluorescence intensity (×10⁵)
6
5
4
3
2
1
0
① ② ③ ④ ⑤
430
450
470
490
510
530
550
570
Wavelength (nm)
g
① ② ③ ④ ⑤
460 nm
530 nm
Overlay

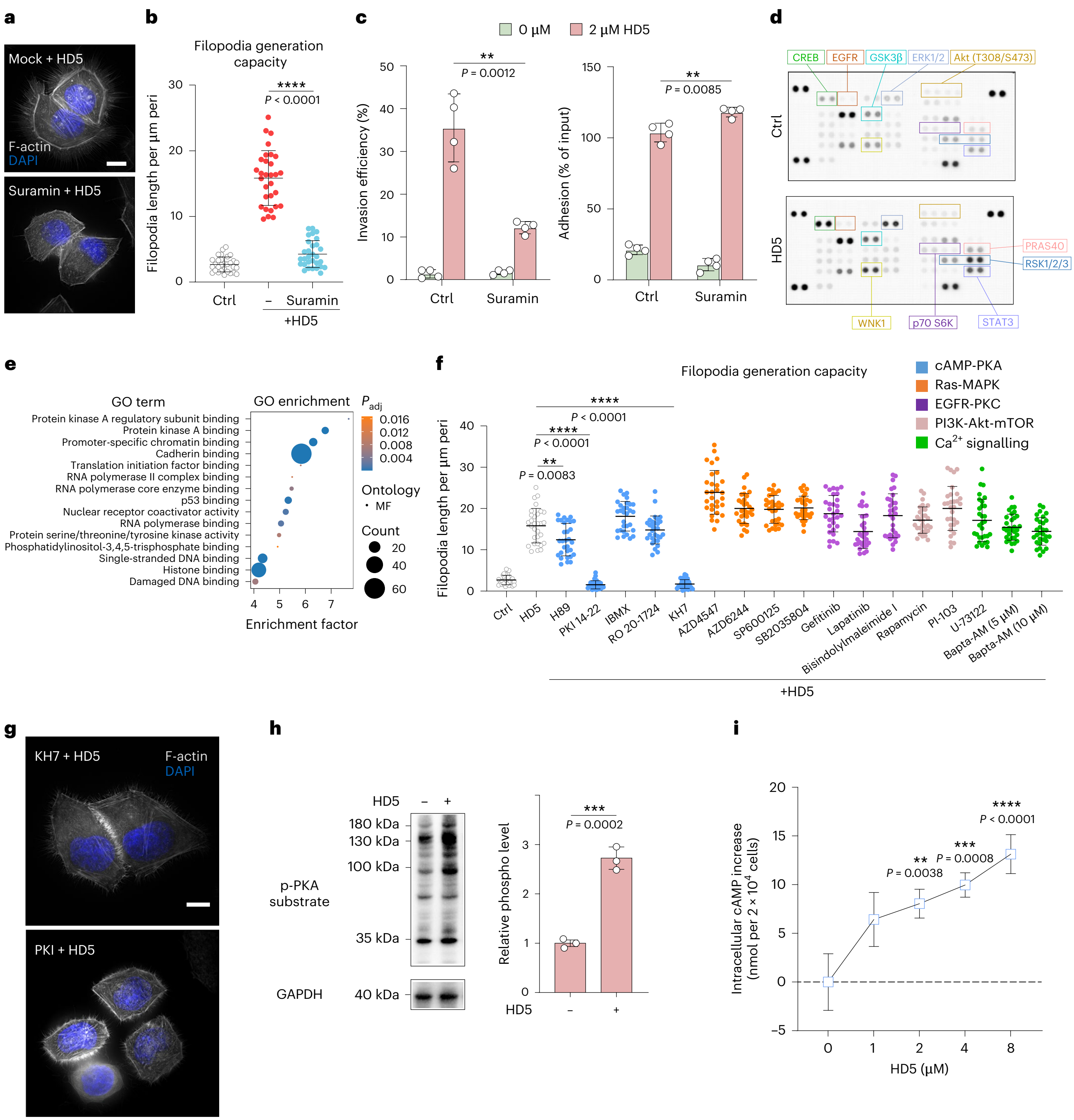

Fig. 3 | HD5 interacts with GPCR to induce HIFE through PKA activation. **a**,**b**, Fluorescence microscopy analysis (**a**) and quantification (**b**) of the influence of suramin on the cytoskeleton of HeLa cells in the presence of 2 µM HD5 ($n = 30$). In **a**, F-actin is grey and nuclei are blue (DAPI). Scale bar, 10 µm. In **b**, data are mean ± s.d. **c**, Influence of 5 µM suramin on the invasion efficiency (left) and adhesion (right) of *Shigella* in the presence or absence of 2 µM HD5 ($n = 4$). Data are mean ± s.d. **d**, Human phosphokinase antibody arrays analysis of HeLa cells upon HD5 stimulation. Significantly altered phosphokinases are framed with different colours. **e**, Top 15 enriched molecular function (MF) terms in the GO enrichment analysis of phosphoproteome. **f**, Quantitative analysis of the influence of different pathway inhibitors on the cytoskeleton of HeLa cells in the presence of 2 µM HD5 ($n = 30$). Data are mean ± s.d. **g**, Fluorescence microscopy examination of GPCR-cAMP-PKA pathway inhibitors on the cytoskeleton of HeLa cells in the presence of 2 µM HD5. F-actin is grey and nuclei are blue (DAPI). Scale bar, 10 µm. **h**, Immunoblotting analysis of PKA activity detected by phospho-(Ser/Thr) PKA substrate antibody (CST, 9624) upon stimulation by 4 µM HD5 for 15 min ($n = 3$). Data are mean ± s.d. **i**, Intracellular cAMP levels in HeLa cells, measured by cAMP-Glo max assay upon stimulation with serial concentrations of HD5 for 15 min ($n = 3$). Data are mean ± s.d. Significance was determined using two-tailed unpaired Student's *t*-test (**b**,**c**,**h**) or one-way ANOVA (with Dunnett's multiple comparisons test) (**f**,**i**); $^{**}P < 0.01$, $^{***}P < 0.001$, $^{****}P < 0.0001$. Results are representative of at least 3 independent experiments.

difference in adhesion level (Fig. 2c). IF analysis showed that HD5-bound *Shigella* established much more entry foci in HD5-primed cells than mock-treated cells within 30 min (Fig. 2c). These results suggest two distinct roles played by HD5 in *Shigella* infection, by acting on the bacterium (to enhance adhesion) and on the host cell (to enhance *Shigella* invasion), respectively (Fig. 2d). To further distinguish these roles, cytochalasin D, an inhibitor of actin polymerization, was introduced into the infection assays, which revealed that while cytochalasin D abolished the formation of HIFE and the subsequent *Shigella* invasion (Fig. 2e), the adhesion-promoting activity of HD5 was barely affected.

We then examined the influence of HD5 upon type III secretion system (T3SS) activation using a Förster resonance energy transfer (FRET) assay[22] (Extended Data Fig. 1d). As revealed in the fluorescence emission spectra and fluorescence microscopic analysis (Fig. 2f,g), blue shifts of the infected cells were significantly accelerated in the 'HD5-bound bacteria plus HD5-primed cell' combination (combination 4). By contrast, pretreatment of *Shigella* (combination 2) or HeLa cells (combination 3) alone did not result in a significant blue shift within 30 min of *Shigella* making contact with the cells. Infection assays using a T3SS-inactivated strain (*ΔmxiD*)[23,24] revealed that while HD5 was capable of promoting adhesion of the *ΔmxiD* mutant, the invasion-enhancing activity of HD5 was only effective for the invasive wildtype strain Sf301 (Extended Data Fig. 1e).

HD5 interacts with GPCR to induce HIFE via PKA activation

Next, HIFE was verified in 10 epithelial cells lines, primary human colonocytes and 8 suspension cell lines (Supplementary Table 1 and Extended Data Fig. 2a), suggesting that cytoskeletal reorganization may be a ubiquitous function of HD5. We then examined whether HD5 exerted this effect inside the cells by microinjection to produce intracellular concentrations of 0.5 to 5 μM, which, however, failed to produce any significant cytoskeletal alteration (Extended Data Fig. 2b). Moreover, addition of 4 μM HD5 into an in vitro actin polymerization system had minimal effect on the nucleation and elongation of actin filaments, excluding the possibility that HD5 exerted its effect intracellularly (Extended Data Fig. 2c). We thus hypothesized that HD5 might instead interact with cell surface components for cytoskeletal reorganization.

α5β1 integrin and CD44, the two receptors previously reported to be involved in *Shigella* invasion[25–27], were first excluded by the finding that genetic depletion of β1 integrin subunit and CD44 from HeLa cells affected neither the association of HD5 with *Shigella* adhesion and invasion, nor the formation of filopodia (Extended Data Fig. 2d–f).

We next considered G protein-coupled receptors (GPCRs) as these have previously been shown to interact with defensins[28–31]. Consistent with this assumption, suramin, a non-specific GPCR inhibitor[32], significantly inhibited HIFE formation (Fig. 3a,b). Notably, suramin decreased the efficiency of *Shigella* invasion from 35.5% to 12.2% in the presence of HD5, without undermining HD5-promote adhesion (Fig. 3c).

To help identify candidate GPCRs, the signalling network induced by HD5 was subjected to human phosphokinase antibody arrays (Fig. 3d and Extended Data Fig. 3a) and system-wide phosphoproteome analysis[33] (Extended Data Fig. 3b). Gene ontology (GO) analysis revealed that multiple cytoskeleton-related GO terms were enriched (Extended Data Fig. 3c), with the top 15 enriched molecular function terms (Fig. 3e) supporting a prominent role for the PKA pathway. This was further verified by the significant antagonizing effect of specific PKA pathway inhibitors PKI 14-22 and KH7, but not any inhibitor against other widely-recognized cytoskeleton-regulating pathways including EGFR, MAPK, PI3K-Akt-mTOR and Ca^{2+} signalling (Fig. 3f,g and Extended Data Fig. 4).

HD5 treatment significantly elevated the activity of PKA by 2.6-fold as detected by phospho-(Ser/Thr) PKA substrate antibody (Fig. 3h), which was further confirmed by the significant increase in intracellular cAMP in HeLa cells (Fig. 3i). The significant phosphorylation of cAMP-responsive element binding protein (CREB), as detected in the phosphokinase antibody arrays, reinforced the activation of the cAMP-PKA pathway (Fig. 3d and Extended Data Fig. 3a).

P2Y11 is identified as the HD5 receptor for HIFE generation

Given the pivotal role of the cAMP-PKA pathway, we assumed that a G protein with either a stimulatory (Gs) or inhibitory (Gi) α-subunit would associate with the GPCR that interacts with HD5. The incompetence of pertussis toxin (PTX), an inhibitor of Gi-coupled receptor signalling[33], in prohibiting HIFE precluded the involvement of a Gi-coupled GPCR. In stark contrast, NF449, a potent Gs α-subunit-selective G-protein antagonist[34], was found to significantly reduce HIFE formation by ~80% (Fig. 4a,b).

We then searched the HGNC database[35] for 1,415 genes known to encode GPCRs. A total of 704 GPCRs were annotated by Reactome (v.86)[36], of which 61 were involved in both 'G alpha (s) signalling events' (R-HSA-418555) and 'GPCRs that activate Gs' (R-HAS-790204). Using RNA-seq, we quantified the expression level for each of these genes in 18 HD5-responsive cell lines, finding that of the 61 candidates, only one was consistently expressed (transcripts per million (TPM) > 1) in every cell line, namely *P2Y11* (Ensembl: ENSG00000244165) (Supplementary Table 1). To corroborate this result, we searched the Human Protein Atlas (v.23.0)[32] for the expression of *P2Y11*, finding detectable expression (nTPM > 1) in each of the cell lines we tested (Fig. 4c, Extended Data Fig. 5a,b and Supplementary Table 1).

Next, we confirmed a direct interaction between HD5 and P2Y11 using a pulldown assay. As shown in immunoblotting analysis (Fig. 4d), specific signals for P2Y11 were observed in proteins pulled down with biotinylated HD5 but not in proteins associated only with beads. Moreover, mass spectrometry analysis confirmed that P2Y11 was specifically present in the HD5-associated protein complex (Extended Data Fig. 5c). The interaction details between HD5 and P2Y11 were computationally validated by molecular docking (Extended Data Fig. 5d) with a binding

Fig. 4 | P2Y11 serves as HD5 receptor to induce HIFE. a,**b**, Fluorescence microscopy analysis (**a**) and quantification (**b**) of the influence of 200 ng ml^{-1} pertussis toxin (PTX) and 40 μM NF449 on the cytoskeleton of HeLa cells in the presence of 2 μM HD5. In **a**, F-actin is grey and nuclei are blue (DAPI). Data in **b** are mean ± s.d. **c**, Illustration of the identification of P2Y11 using transcriptome data, Reactome and the Human Protein Atlas database. **d**, Immunoblotting analysis of protein samples pulled down by biotin-HD5 using P2Y11 antibody. **e**, Molecular dynamics (MD) simulation (100 ns) of the interaction between HD5 and P2Y11. The two monomers of HD5 were coloured with fuchsia and green, respectively; and the hydrogen bonds were indicated with yellow dashed lines. Residues contributing hydrogen bonds were highlighted as stick models with nitrogen atoms coloured blue, oxygen atoms coloured red, and carbon atoms from the two monomers of HD5 and P2Y11 coloured fuchsia, green and white, respectively. **f**,**g**, Fluorescence microscopy analysis (**f**) and quantification (**g**) of the influence of NF157 and NF340 on the cytoskeleton of HeLa cells in the presence of 2 μM HD5 ($n = 30$). In **f**, F-actin is grey and nuclei are blue (DAPI). Scale bar, 10 μm. In **g**, data are mean ± s.d. **h**, MD simulation of the influence of the interaction between NF157 and P2Y11. NF157 and P2Y11 residues contributing hydrogens bonds were highlighted as stick models with nitrogen atoms coloured blue, oxygen atoms coloured red, sulfur atoms coloured yellow, and carbon atoms from NF157 and P2Y11 coloured cyan and white, respectively; the hydrogen bonds were indicated with yellow dashed lines. **i**–**k**, Fluorescence microscopy analysis (**i**) and quantification (**j**,**k**) of parental and *P2Y11*-knockout HeLa cells in the presence of 2 μM HD5 ($n = 30$). In **i**, F-actin is grey and nuclei are blue (DAPI). Scale bar, 10 μm. In **j** and **k**, data are mean ± s.d. Significance was determined using two-tailed unpaired Student's *t*-test (**j**,**k**) or one-way ANOVA (with Dunnett's multiple comparisons test) (**b**,**g**); $^{**}P < 0.01$, $^{***}P < 0.001$ and $^{****}P < 0.0001$. Results are representative of at least 3 independent experiments. Reactome logo reproduced under a Creative Commons licence CC BY 4.0.

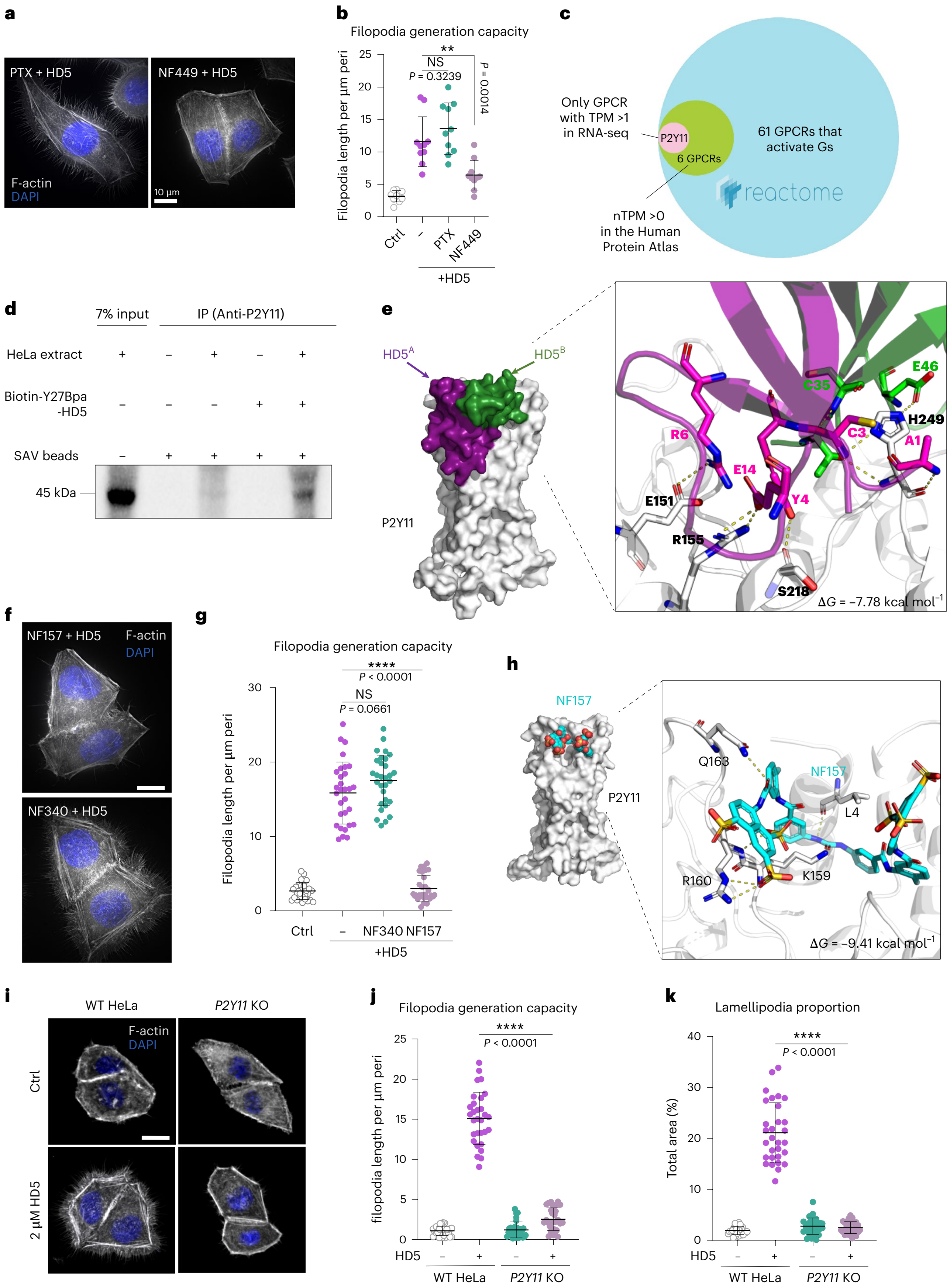
a
PTX + HD5
NF449 + HD5
F-actin
DAPI
10 µm
b
Filopodia generation capacity
Filopodia length per µm peri
25
20
15
10
5
0
**
NS
P = 0.3239
P = 0.0014
Ctrl
–
PTX
NF449
+HD5
c
Only GPCR with TPM >1 in RNA-seq
P2Y11
6 GPCRs
61 GPCRs that activate Gs
reactome
nTPM >0 in the Human Protein Atlas
d
7% input
IP (Anti-P2Y11)
HeLa extract
+ – + – +
Biotin-Y27Bpa -HD5
– – – + +
SAV beads
– + + + +
45 kDa
e
HD5A
HD5B
P2Y11
E46
C35
H249
R6
C3
A1
E14
E151
Y4
R155
S218
ΔG = –7.78 kcal mol−1
f
NF157 + HD5
F-actin
DAPI
NF340 + HD5
g
Filopodia generation capacity
Filopodia length per µm peri
30
20
10
0
****
P < 0.0001
NS
P = 0.0661
Ctrl
–
NF340
NF157
+HD5
h
NF157
P2Y11
Q163
NF157
L4
R160
K159
ΔG = –9.41 kcal mol−1
i
WT HeLa
P2Y11 KO
F-actin
DAPI
Ctrl
2 µM HD5
j
Filopodia generation capacity
filopodia length per µm peri
25
20
15
10
5
0
****
P < 0.0001
HD5
– + – +
WT HeLa
P2Y11 KO
k
Lamellipodia proportion
Total area (%)
40
30
20
10
0
****
P < 0.0001
HD5
– + – +
WT HeLa
P2Y11 KO

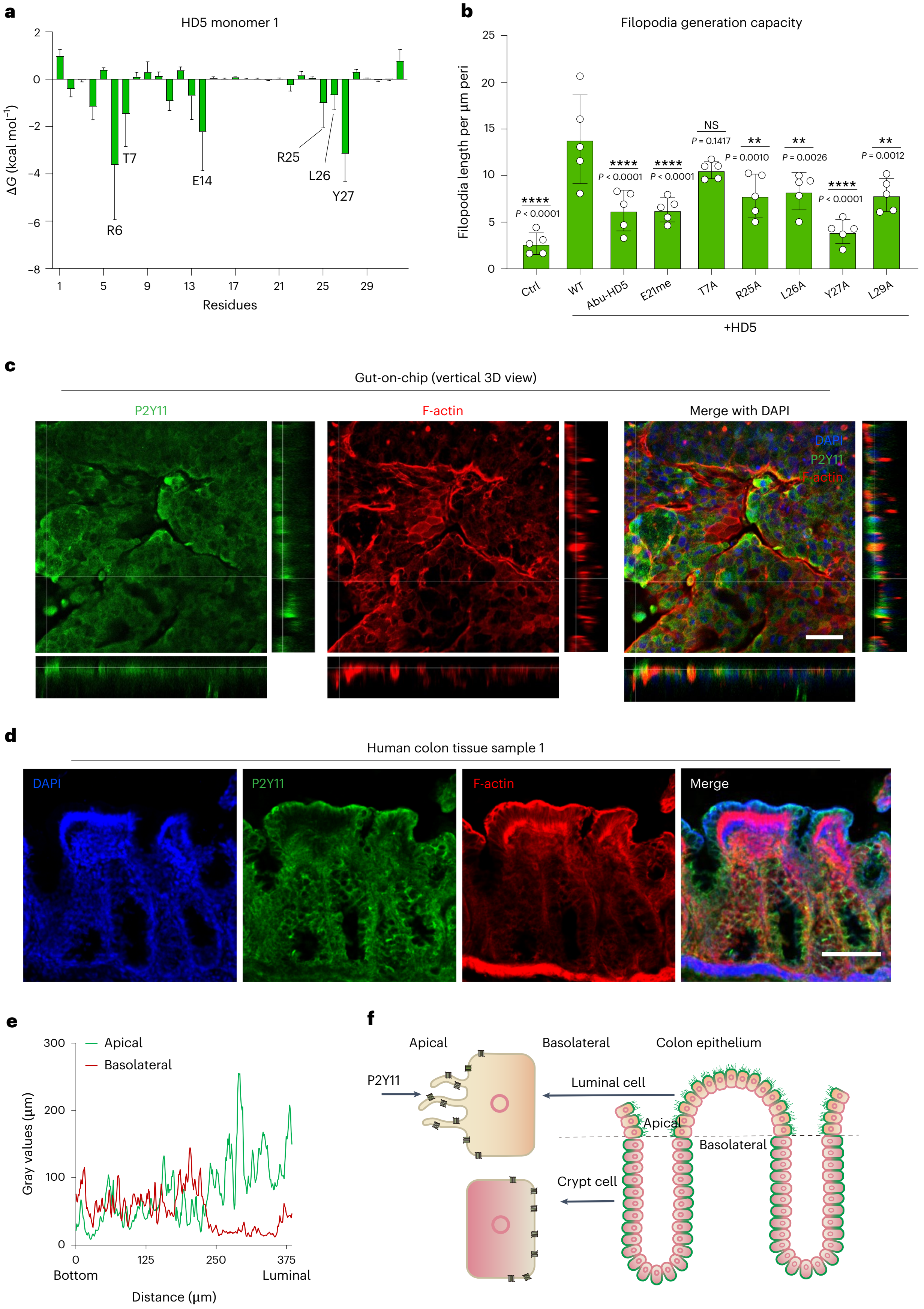
a
HD5 monomer 1
ΔG (kcal mol^{-1})
2
0
−2
−4
−6
−8
R6
T7
E14
R25
L26
Y27
1
5
9
13
17
21
25
29
Residues
b
Filopodia generation capacity
Filopodia length per μm peri
25
20
15
10
5
0
****
P < 0.0001
****
P < 0.0001
****
P < 0.0001
NS
P = 0.1417
**
P = 0.0010
**
P = 0.0026
****
P < 0.0001
**
P = 0.0012
Ctrl
WT
Abu-HD5
E21me
T7A
R25A
L26A
Y27A
L29A
+HD5
c
Gut-on-chip (vertical 3D view)
P2Y11
F-actin
Merge with DAPI
DAPI
P2Y11
F-actin
d
Human colon tissue sample 1
DAPI
P2Y11
F-actin
Merge
e
Apical
Basolateral
Gray values (μm)
300
200
100
0
0
125
250
375
Bottom
Luminal
Distance (μm)
f
Apical
Basolateral
Colon epithelium
P2Y11
Luminal cell
Apical
Basolateral
Crypt cell

Fig. 5 | Critical residues of HD5 for interaction with P2Y11 and the distribution pattern of P2Y11 in gut-on-chip and human colonic tissue. a, Prediction of critical residues of HD5 monomer 1 for interaction with P2Y11 by MD simulation. Each amino acid mean was generated from 2,500 raw data points. Data are mean ± s.d. **b**, Quantification of the influence of wildtype HD5 and its mutants on the cytoskeleton of HeLa cells at the concentration of 2 μM ($n = 5$). Data are mean ± s.d. Significance was determined using one-way ANOVA (with Dunnett's multiple comparisons test); $**P < 0.01$, $****P < 0.0001$. **c**, Fluorescence microscopy analysis of P2Y11 distribution in gut-on-chip built with CACO-2 cells. Vertical 3D view with two side views is shown. P2Y11 is green, F-actin is red and nuclei are blue (DAPI). Scale bar, 50 μm. **d**, Fluorescence microscopy analysis of P2Y11 distribution in human colonic tissue in human tissue sample. P2Y11 is green, F-actin is red and nuclei are blue (DAPI). Scale bar, 100 μm. **e**, Gray values of P2Y11 signals in the apical and basolateral regions in human colonic crypt. **f**, Graphic illustration of the bimodal distribution of P2Y11 in human colonic epithelium. Results are representative of at least 3 independent experiments.

free energy of −7.78 kcal mol^{-1} (Fig. 4e), contributed mainly by stable interactions including hydrogen bonds and electrostatic forces.

The involvement of P2Y11 in interacting with HD5 was then examined using two P2Y11-specific antagonists, NF340 and NF157 (refs. 37,38). Intriguingly, NF340 (ref. 39) barely affected the cytoskeleton-rearranging activity of HD5, while NF157, occupying different binding amino acid residues from those of NF340 (ref. 40), effectively abolished HIFE (Fig. 4f,g). To address this discrepancy, NF340 and NF157 were also subjected to the MD simulation, which showed that NF157 fit well with the receptor pocket in which HD5 bound, contributing an even stronger binding affinity (−9.41 kcal mol^{-1}), in contrast with the weaker affinity of NF340 (−2.99 kcal mol^{-1}) (Fig. 4h and Extended Data Fig. 5e). Moreover, the observation that NF157, even added after HD5, still attenuated the effect of HD5 on the cytoskeleton reinforced the higher binding affinity of NF157 (Extended Data Fig. 5f,g).

More importantly, while CRISPR/Cas9 knockout (KO) of the *P2Y11* gene from HeLa cells did not influence the basal filopodia and lamellipodia, upon stimulation with HD5, the filopodia generation capacity and lamellipodial proportion of *P2Y11*-KO cells decreased by 66% and 84%, respectively (Fig. 4i–k and Extended Data Fig. 5h).

Notably, two known P2Y11 ligands, ATPγs and NAD$^+$, did not induce HIFE-like structures or promote *Shigella* infection (Extended Data Fig. 6a,b), suggesting that the interaction between HD5 and P2Y11 differs from that with the known agonists. Furthermore, a Caspase-Glo assay showed that up to 20 μM NF157 did not reduce cell apoptosis caused by HD5 in both non-infected and infected conditions, indicating that, unlike its filopodia-stimulating effect, HD5 probably exerted its apoptotic effect in an NF157-independent way, not necessarily mediated through P2Y11 signalling (Extended Data Fig. 6c).

Critical residues of HD5 for interaction with P2Y11

A steady-phase trajectory for Molecular Mechanics/Generalized Born Surface Area (MM/GBSA) free energy (ΔG) calculation, derived from a 100-ns MD simulation, dissected the critical determinants of HD5 for generating HIFE (Extended Data Figs. 5d and 7a), showing that the R6, T7, E14, R25, L26 and Y27 residues of monomer 1 of HD5, but not any residue of monomer 2, contributed the major binding free energy to engage the receptor (Fig. 5a).

To validate the prediction by MD simulation, a series of substitution HD5 mutants were chemically made. Since R6 and E14 formed a salt bridge that was structurally essential, we assumed that the native tertiary conformation of HD5 was indispensable. This was verified by the total function loss of the lineated HD5 mutant after replacement of six Cys residues by isosteric aminobutyric acid (Abu)[41] to remove the three intramolecular disulfide bonds. The pivotal role of Y27 was validated since the Y27A mutant was functionally detrimental. Moreover, alanine substitutions at R25 and L26 exhibited slightly reduced activity in generating HIFE (Fig. 5a,b). We also noted that the predicted contribution of T7 was not reflected experimentally.

Since the Y27A-HD5 mutant was previously found to exist as a monomer but not a dimer (unlike wildtype HD5)[5], we then examined whether dimerization of HD5 was required for its cytoskeleton-reorganizing activity by creating a dimerization-debilitating analogue E21Me-HD5, where the amide peptide bond was methylated at Glu21 (ref. 41). HIFE analysis revealed that E21Me-HD5 was largely inactive in inducing HIFE (Fig. 5b). Moreover, alanine substitution scanning also uncovered the importance of L29 (Fig. 5b), which has previously been considered essential for stabilizing the hydrophobic core of the defensin molecule[41], in conveying the cytoskeleton-reorganizing activity of HD5.

Collectively, our results emphasized that to interact with P2Y11 and induce HIFE, the native tertiary conformation, dimerization, selective cationic residues and hydrophobicity of HD5 were indispensable.

P2Y11 is apically distributed on human colonic epithelium

While P2Y11 was found to be evenly distributed on the surface of HeLa cells and along the newly-formed HIFE (Extended Data Fig. 7b), a gut-on-chip model demonstrated an apical distribution of the receptor on the luminal surface of the colonic epithelial surface (Fig. 5c). More importantly, in human colonic tissue sections, P2Y11 was generally expressed in the human colonic epithelial layer, consistent with its tissue distribution in the Human Protein Atlas. Moreover, our IF analysis revealed that P2Y11 was differentially distributed along the human colon crypts (Fig. 5d and Supplementary Video 4). Particularly, in the differentiated enterocytes on the luminal epithelial surface, P2Y11 was located exclusively at the apical membrane, with little or no basolateral staining, whereas in the lower part of colonic crypts, P2Y11 showed stronger signals along the basolateral regions of the cells (Fig. 5e,f and Extended Data Fig. 7c). Collectively, our data support the physiological precondition of bona fide interaction between P2Y11 and HD5.

Moreover, the physiological implications of the cytoskeleton-regulating effect of HD5–P2Y11 interaction beyond its pathogenic role in *Shigella* infection were confirmed by its activities in promoting initial

Fig. 6 | Intervention of P2Y11 prevented the HD5-faciliated *Shigella* invasion. a, Effect of NF157 on *Shigella* invasion efficiency in HeLa cells ($n = 4$). **b**, Fluorescence microscopy analysis of the influence of 20 μM NF157 on TSAR activation of Sf301 in HeLa cells in the presence of 2 μM HD5. HeLa cells are counterstained with DAPI, F-actin is grey, *Shigella* bacteria are red, and GFP expression is induced upon activation of the type 3 secretion system. Scale bar, 10 μm. Right: green/red ratio ($n = 5$). **c**–**e**, Influence of 20 μM NF157 on *Shigella* infection of polarized primary colonocytes monolayer derived from human colonic organoids. **c**, Fluorescence microscopy analysis. F-actin is grey, bacteria are red and nuclei are stained with DAPI (blue). Scale bar, 100 μm. **d**, Infection area of the polarized primary colonocytes monolayer ($n = 5$). **e**, Transepithelial electrical resistance (TEER) of polarized primary colonocytes monolayer ($n = 3$). **f**, Invasion efficiency of *Shigella* on *P2Y11*-knockout (*P2Y11*-KO) HeLa cells. P2Y11 expression was rescued from the KO cells by *P2Y11* knock-in (*P2Y11* KO + KI) ($n = 4$). **g**, Fluorescence microscopy analysis of *Shigella* invasion of *P2Y11*-KO HeLa cells in the presence of 2 μM HD5. GFP-expressing bacteria are green, F-actin is red and nuclei are blue (DAPI). White arrows, actin foci of active *Shigella* invasion. Scale bar, 20 μm. **h**,**i**, Influence of 20 μM NF157 on *Shigella* infection of gut-on-chip. In **h**, F-actin is red, actively-invading bacteria are green (TSAR-positive) and nuclei are stained with DAPI (blue). Scale bar, 50 μm. **i**, TSAR-positive area ($n = 3$). **j**, Influence of NF157 on Serény test using guinea pigs ($n = 20$). Data points represent inflammation scores of animals. Significance was determined using two-tailed unpaired Student's t-test (**a**,**b**,**e**), one-way ANOVA (with Tukey's multiple comparisons test) (**d**,**f**,**i**) or Mann–Whitney test (**j**); $*P < 0.05$, $**P < 0.01$, $***P < 0.001$, $****P < 0.0001$. Data are mean ± s.d. (**a**,**b**,**d**–**f**,**i**). Results are representative of at least 3 independent experiments.

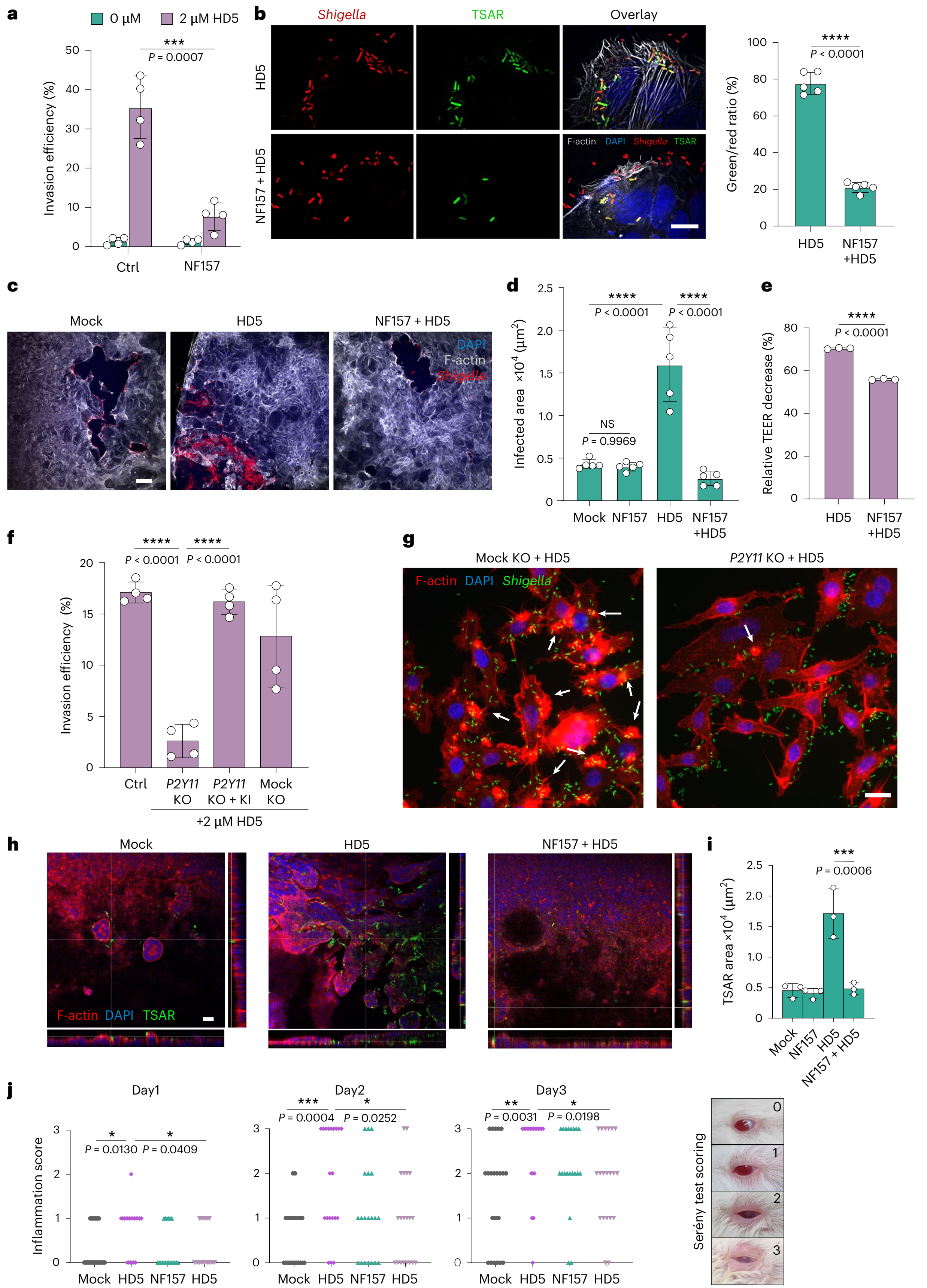
a
0 µM
2 µM HD5
***
P = 0.0007
Invasion efficiency (%)
0
10
20
30
40
50
Ctrl
NF157
b
Shigella
TSAR
Overlay
HD5
NF157 + HD5
F-actin DAPI Shigella TSAR
Green/red ratio (%)
0
20
40
60
80
100
****
P < 0.0001
HD5
NF157 +HD5
c
Mock
HD5
NF157 + HD5
DAPI
F-actin
Shigella
d
Infected area ×10^4 (µm^2)
0
0.5
1.0
1.5
2.0
2.5
****
P < 0.0001
****
P < 0.0001
NS
P = 0.9969
Mock
NF157
HD5
NF157 +HD5
e
Relative TEER decrease (%)
0
20
40
60
80
****
P < 0.0001
HD5
NF157 +HD5
f
Invasion efficiency (%)
0
5
10
15
20
****
P < 0.0001
****
P < 0.0001
Ctrl
P2Y11 KO
P2Y11 KO + KI
Mock KO
+2 µM HD5
g
Mock KO + HD5
P2Y11 KO + HD5
F-actin DAPI Shigella
h
Mock
HD5
NF157 + HD5
F-actin DAPI TSAR
i
TSAR area ×10^4 (µm^2)
0
0.5
1.0
1.5
2.0
2.5
***
P = 0.0006
Mock
NF157
HD5
NF157 + HD5
j
Day1
Day2
Day3
Inflammation score
0
1
2
3
*
P = 0.0130
*
P = 0.0409
***
P = 0.0004
*
P = 0.0252
**
P = 0.0031
*
P = 0.0198
Mock
HD5
NF157
HD5 +NF157
Serény test scoring
0
1
2
3

cell attachment, CACO-2 cell polarization along with concomitant generation of microvilli, and remarkably, a non-negligible contribution to the apparent integrity of the intestinal barrier upon 10% dextran sulfate sodium (DSS) damage (Extended Data Fig. 8).

P2Y11 activation accounts for HD5-mediated *Shigella* invasion

To validate a causal link between HD5-induced P2Y11 activation and enhanced *Shigella* infection, we examined bacterial invasion with respect to P2Y11 interventions in in vitro, organoid, dynamic gut-on-chip and in vivo models.

First, while NF157 per se did not influence the spontaneous bacterial adhesion and invasion in the absence of HD5 (Extended Data Fig. 9a), it significantly reduced the invasion/adhesion ratio of already-adhering *Shigella* bacteria in the presence of HD5 in both epithelial cells (HeLa and CACO-2) and phorbol myristate acetate (PMA)-differentiated THP-1 macrophages (Fig. 6a and Extended Data Fig. 9b–d). Microscopic analysis of T3SS secretion activity using a type 3 secretion activation reporter (TSAR) system assay[42] revealed that NF157 significantly reduced the green/red ratio of the adhering TSAR-containing bacteria in HeLa and CACO-2 cells (Fig. 6b and Extended Data Fig. 10a). Second, polarized epithelial monolayers of primary human colonocytes (from human organoids) were used to examine the effect of NF157 on *Shigella* invasion. While the presence of 4 μM HD5 increased *Shigella* infection in the whole monolayer after a 3-h infection, the addition of 20 μM NF157 significantly reduced the bacterial infection area on the primary colonocyte monolayer by 3.7-fold (Fig. 6c,d). Concomitantly, the TEER drop due to epithelial destruction was also counteracted by NF157 (Fig. 6e). Similar results were obtained in polarized CACO-2 cells, as evidenced by an 89% decrease in intracellular bacteria, TEER rescue and alleviated epithelial destruction (Extended Data Fig. 10b–d).

Moreover, while *P2Y11* knockout per se did not influence spontaneous *Shigella* infection, invasion promoted by HD5 was much less pronounced in the *P2Y11*-KO cells, with an invasion/adhesion ratio of 3% in 30 min compared with 17% in parental or mock KO HeLa cells in the presence of HD5. More importantly, upon P2Y11 expression rescue, *Shigella* showed a significantly elevated invasion efficiency in the presence of HD5 (Fig. 6f). Fluorescence analysis further demonstrated that in *P2Y11*-KO cells, fewer HIFE were generated upon stimulation by HD5, reducing bacterial capture and subsequent formation of actin foci that are indicative of active bacterial invasion (Fig. 6g).

A gut-on-chip model was subjected to *Shigella* infection with a constant flow rate of 20 μl h^{-1}. While the presence of HD5 greatly promoted the aggregation of the bacterial cells and the formation of substantial active invasion loci (as indicated by pronounced TSAR activity) predominantly in the crypt-like structures of the gut-on-chip (as reported previously[43]), NF157 significantly decreased the size and number of bacterial clusters (Fig. 6h,i, Extended Data Fig. 10e and Supplementary Videos 5–8).

More critically, the in vivo effect of NF157 was verified using a Serény test on guinea pigs. Expression of P2Y11 and its binding with HD5 on the corneal epithelia of guinea pigs was confirmed (Extended Data Fig. 10f). While HD5 significantly potentiated keratoconjunctivitis with the bacterial inoculum of 1×10^6 colony-forming units (c.f.u.s) per eye all after 3 days, administration of NF157 significantly ameliorated HD5-augmented infection at all time points (Fig. 6j).

Discussion

We have shown that HD5 stimulates the formation of filopodial extensions on the surface of colonic epithelial cells by acting on its receptor P2Y11; these extensions are exploited by *Shigella* to facilitate its capture and subsequent invasion. Supporting the biological plausibility of this mechanism, we note that despite a documented small intestinal origin of HD5, its immunohistochemical detection in colon biopsies suggests that local production is possible[44]. Moreover, HD5 has also been found at low micromolar concentrations in ileal aspirates collected at the junction between the ileum and the proximal colon, consistent with luminal migration[5,45,46].

We have identified P2Y11 as the HD5 receptor for this activity. Although the functions of human alpha defensins have been extensively documented[3,4,47–49], to the best of our knowledge, no bona fide receptor had so far been identified for HD5, largely on account of their promiscuous binding behaviours[47,50]. Successful identification of a specific human defensin receptor has previously only been achieved for beta defensins[28,30,51], although these are both structurally and functionally distinct[1,2,47,52].

Although we characterize P2Y11 as a specific HD5 receptor, it is no surprise that it is a GPCR—virtually all receptors known to interact with defensins, both human and murine, belong to this family[28,30,31,51] (with one exception, TLR4, for murine β-defensin 2 (ref. 53)). Although documented as a purinergic receptor, P2Y11 differs from its family members in several respects. First, it is the only known Gs protein-coupled purinergic receptor that directly modulates intracellular cAMP level and PKA activity[53,54], which is reported to be involved in the polarization and migration of T lymphocytes[55]. Second, besides ATP, it also uses other endogenous factors, such as the dinucleotide NAD^+, as a ligand to initiate a cellular response, especially in immune cells[56]. It is therefore not unexpected that the cAMP-PKA pathway activated downstream of P2Y11–HD5 interaction would lead to HIFE since previous studies suggest a pivotal role of cAMP-PKA both in cytoskeletal reorganization and filopodial generation in a range of human cells[57–59]. Nevertheless, whether HD5 plays an active role in the bimodal distribution of P2Y11 along the colonic epithelial crypt, as found in this study, warrants further investigation.

In summary, these results further our understanding of the mechanistic basis of HD5-augmented pathogen infection and open the possibility for novel intervention strategies against pathogens that exploit HD5-induced filopodial extensions.

Methods

Ethics approval

The study was completely conducted in compliance with the appropriate ethics guidelines and regulations. The animal studies were approved by the Biomedical Ethics Committee of the Health Science Center of Xi'an Jiaotong University (Ethics approval no. XJTUUAE2024-2007). The use of human colonic tissues for P2Y11 expression analysis was approved by the Ethics Committee of the Hospital of Stomatology of Xi'an Jiaotong University (Ethics approval no. 2024-XJKQIEC-QT-0026-001). Informed consent was obtained from the guardians of all tissue donors.

Reagents

All peptides used in this study were chemically synthesized, correctly folded and highly purified as previously described[54–56,60]. A detailed list of all oligonucleotide sequences and commercial reagents is provided in the resources and reagents table (Supplementary Table 1).

Cell lines

All cell lines were passaged for fewer than 6 months and were characterized by DNA fingerprinting analysis[59]. All cell lines were tested for mycoplasma and were found to be free from infection. U-937, THP-1, K-562, Jurkat, D5, D6, F7 and M8 cells were maintained in RPMI-1640 medium supplemented with 10% certified fetal bovine serum (BI, C04001-500) and 1% penicillin/streptomycin solution, whereas A-549, CACO-2, Hep-G2, HT-29, MCF-7, MS751, PC-3, SiHa, HEK293T and HeLa cells were maintained in DMEM medium supplemented with 10% fetal bovine serum (FBS) and 1% penicillin/streptomycin solution. All cell lines were grown in 5% CO_2 under a water-saturated atmosphere in a cell incubator at 37 °C. For HIFE inhibition, cells were pretreated with inhibitors for 30 min.

In vitro adhesion and invasion assays on cell lines

The cell lines and their culture media used in this study are listed in Supplementary Table 1. One day before the assays, cells were seeded into 24-well plates at a density of ~10^5 cells per well. Before infection, cells were washed in serum-free medium, and HD5 at indicated concentrations was added into the medium while adding ~10^6 c.f.u.s of Sf301 from mid-exponential phase. Bacteria were centrifuged (500 *g*, 10 min, r.t.) onto HeLa cells (MOI 10:1, or indicated MOI) to synchronize the infection. For the adhesion assay, after thorough washing, cells were lysed with 1 ml sterile water per well for 20 min and diluted with PBS. The c.f.u.s were enumerated after plating. For the invasion assay, bacteria/HeLa mixtures were incubated for 30 min after centrifugation and then washed, treated with gentamicin-containing (100 μg ml^{-1}) medium for another 20 min before lysis for plating. Adhesion was defined as the total number of cell-associated bacteria and is shown as the percentage of input. Invasion was defined as the total number of intracellular bacteria in cells (extracellular bacteria were killed by gentamicin, a cell-impermeable antibiotic). For separate pretreatment of *Shigella* (HD5-bound Sf301) and HeLa cells (HD5-primed HeLa cells), both were incubated with 2 μM HD5 for 15 min, followed by thorough washing (three times) to remove the unbound HD5 to generate HD5-bound Sf301 and HD5-primed HeLa cells, respectively. A schematic illustration of the assays is shown in Extended Data Fig. 1c.

Primary human colonocytes culture and *Shigella* infection procedure

Primary human colonocytes were cultured in vitro. Briefly, human colonoids were commercially generated by D1 Medical Technology company. The company has a dedicated team that procures both research and cGMP-grade tissue according to the highest ethical standards and in compliance with government regulations (Ethics approval no. 050432-4-1212B). Primary colonocytes were isolated, seeded in Matrigel and cultured with organoid culture medium as instructed by the manufacturer[61]. Colonoids between ~5 and 25 passages were used for further experiments. Human colonocytes were obtained from the mechanical and enzymatic dissociation of colonoids and were plated for HD5 stimulation and, later, immunofluorescence assay. To get access to the lumen surface of the colonoid for TEER measurement and bacterial infection, two-dimensional (2D) human colonoid monolayers were generated on Transwell[62]. Formation of an intestinal barrier due to colonocyte polarization and differentiation in our system was confirmed by a steady increase and maintenance of TEER (over 500 Ω cm^2) as measured by a Millicell ERS-2 voltohmmeter (Merck Millipore) within a 2-week culture. For the invasion assay, the human colonoid monolayers in Transwell were rinsed in a serum-free medium and ~10^7 c.f.u.s of Sf301 from the mid-exponential phase were added in the absence or presence of NF157/HD5. Bacteria were allowed to infect the monolayer (MOI 100:1) for 3 h (without centrifugation). TEER values and bacterial fluorescence were used to quantify infection.

Infection of polarized CACO-2 cells

CACO-2 cells (5×10^4 cells per well) were grown on 24-well Transwell inserts with a 0.4 μm pore size (Corning), in 10% FBS DMEM. At 14 days after seeding, cells were polarized with TEER over 500 Ω cm^2. After rinsing with serum-free DMEM, Sf301 bacteria at MOI = 100:1 were added to the apical chamber with or without HD5/NF157. Bacteria/HeLa mixtures were incubated for 6.5 h, washed and then treated with gentamicin-containing (100 μg ml^{-1}) medium for 30 min. TEER values of the polarized epithelial monolayer were monitored hourly for 7 h.

Serény test

The 6–8-week-old female pathogen-free Hartley guinea pigs used in this study were acquired from the Experimental Animal Center of Xi'an Jiaotong University. We complied with all relevant ethics regulations. During the experiment, 20 healthy guinea pigs were assigned randomly to each group (80 animals in total) and their eyes were rinsed with DMEM before inoculation of Sf301. The NF157 groups were pretreated with 20 μM NF157 for 30 min. Eyes were inoculated with 10^6 c.f.u.s per eye of mid-log phase Sf301 *Shigella* in the absence and presence of 4 μM HD5. Animals were observed and scored for three consecutive days for the development of conjunctivitis and classified according to the degree of inflammation. Eye pathology was scored on a scale of 0–3: Grade 0 (no disease or mild irritation), Grade 1 (mild conjunctivitis or late development and/or rapid clearing of symptoms), Grade 2 (keratoconjunctivitis without purulence) and Grade 3 (fully developed keratoconjunctivitis with purulence).

Gut-on-chip model and *Shigella* infection procedure

The fabrication of the gut-on-chip device builds upon our previous work and involves the development of a microfluidic device with upper and lower chambers separated by a porous membrane[57]. Briefly, a 250-μm-thick silicone sheet (Rogers) and a porous polyester membrane (AR Brown) were cut using a laser cutter (Epilog Laser) and cleaned with 70% isopropyl alcohol (Fisher Scientific). The porous polyester membrane had a pore size of 0.4 μm, pore density of 4×10^6 pores per cm^2 and thickness of 10 μm. The porous membrane was then bonded to the upper PDMS device (single upper chamber) using SYLGARD 184 Silicone Elastomer (Dow Chemical) containing a silicone elastomer base and curing agent, and cured at a constant temperature of 55 °C overnight. Subsequently, it was bonded to the lower PDMS device block using a plasma cleaner. The resulting devices included a top chamber with volume of ~1 μl (length × width × height: 10 mm × 1 mm × 100 μm) and a bottom chamber with volume of ~2.5 μl (length × width × height: 10 mm × 1 mm × 250 μm). In another layer of PDMS, circular holes with a diameter of 8 mm were made with a hole punch. This was then bound to the upper chamber with a plasma cleaner and used as a top cover for adding culture medium. The device chambers were cleaned and sterilized with 70% ethanol, followed by rinsing with sterile water, injecting with air to remove any residual liquid and exposing the device's surface to UV light for 30 min on each side.

Human CACO-2 (intestinal epithelial) cells were cultured in a cell culture flask with DMEM containing 10% of FBS and 1% penicillin/streptomycin. Before seeding CACO-2 cells into the device, the chip was first coated with 10 μg ml^{-1} poly-L-lysine and incubated at 37 °C for 30 min, followed by 3 washes with PBS, each lasting 5 min. Subsequently, it was coated with a 50 μg ml^{-1} solution of bovine plasma fibronectin (Gibco) at 37 °C for 30 min and finally coated with a mixed solution of Matrigel (50 μg ml^{-1}) and Type I Collagen (100 μg ml^{-1}) (BD) at 37 °C for 30 min. All chips were stored at 4 °C and used within 48 h. CACO-2 cells were seeded at a concentration of 8×10^6 cells per ml in the upper channel statically for 4 h at 37 °C and 5% CO_2 in the DMEM/LOW complete medium. The same fresh cell culture medium was perfused at the rate of 20 μl h^{-1} on top of cells for the next 3 days.

To carry out *Shigella* infection in the gut-on-chip, the chips were washed for 4 h at 20 μl h^{-1} in regular cell culture media without antibiotics in both channels. Then, cells were pretreated with NF157 (20 μM) for 30 min, and HD5 (4 μM) was added 15 min later and flowed for another 15 min. In this experiment, *Shigella* Sf301-GFP was used for infection at an MOI of 1:1. Bacteria were also pretreated with HD5 (4 μM) for 15 min before being added to the cells and dynamic infection conducted for 2 h with a flow rate of 20 μl h^{-1}. Infection was stopped by treating with 100 μg ml^{-1} gentamicin for 30 min at a speed of 30 μl h^{-1}. Chips were immediately fixed with 4% paraformaldehyde for immunofluorescence.

Human colonic tissue collection, preparation and storage

Five candidates, two males and three females, aged 2–11 months and diagnosed with congenital megacolon, were recruited randomly from the Affiliated Children's Hospital of Xi'an Jiaotong University for the collection of colonic tissues from congenital megacolon ostomy. There were no self-selection bias or other bias. The study details were fully disclosed by clinicians and researchers for recruitment purposes. The colonic tissues were collected from surgically removed specimens of congenital megacolon ostomy within 1 h of resection. Routine procedures were followed, which included thorough rinsing with PBS and immediate embedding in Tissue-Tek OCT compound (Sakura) using a flash-freeze protocol. The samples were then frozen at −80 °C for further analysis.

Time-lapse microscopic analysis of the cytoskeleton alteration of HeLa cells

HeLa cells were plated the preceding day on 35 mm glass-bottom dishes that were tissue-culture treated. Cells were rinsed three times in DMEM, followed by replacement with staining solution containing 200 nM SiR-actin, a live-cell fluorogenic F-actin labelling probe (Spirochrome, CY-SC001). Live cells were then stained in the incubator at 37 °C in a humidified atmosphere containing 5% CO_2 for 4–6 h. Cells were then mounted in a 37 °C microscope chamber. Wide-field fluorescence microscopy analysis was performed on cells upon HD5 or mock treatment with an Opterra swept-field confocal microscope (Bruker) equipped with a thermic chamber and CO_2 control. Images were acquired every 30 s and analysed using Fiji 2.0.0 software.

Förster resonance energy transfer assay

HeLa cells loaded with the FRET probe CCF4-AM cleavable by β-lactamase (Bla) were infected with *Shigella* carrying a reporter gene of *bla* fused with *ipgD* that encodes the T3SS effector protein IpgD[17]. The FRET of the infected cells in combinations of different treatments for infection was analysed by confocal fluorescence microscopy and fluorescence emission spectra analysis. A blue shift of the fluorescence emission is indicative of the secreting activity of T3SS.

Transcriptional secretion activation reporter system of T3SS

To monitor the activation of T3SS during the bacterial invasion of host cells, invasion assay was carried out with mCherry-labelled wildtype Sf301 harbouring a GFP-expressing reporter plasmid[40] for 30 min or the indicated time period. GFP expression was induced upon activation of the T3SS triggered by bacterial cell contact with the host. CR/HD5-treated bacteria or infected cells were fixed for 15 min in 4% paraformaldehyde at room temperature and permeabilized in PBS-Triton X-100 0.1%, blocked in 1% BSA and washed in PBS following regular immunofluorescence procedure.

Pyrene assay of in vitro actin polymerization

Actin (4 µM, labelled with pyrene) was polymerized in the presence of 1 nM formin or 4 µM HD5 at 22 °C in F-buffer (5 mM Tris-HCl, pH 7.8, 1 mM $MgCl_2$, 0.2 mM EGTA, 0.2 mM ATP, 1 mM dithiothreitol, 50 mM KCl). As soon as the actin was added, the mix was placed in quartz cuvettes and analysed for fluorescence signal for at least 30 min. Actin polymerization was measured by tracking pyrene fluorescence (excitation at 365 nm and emission at 407 nm) on a fluorescence spectrophotometer (Agilent) for 2,400 s at 22 °C.

Phosphoproteomic analysis

Cells with 50% confluence were treated with 4 µM HD5 in the presence or absence of suramin. Proteins were extracted using ice-cold 8 M urea and subjected to further analysis. Trypsin-digested peptides were first dissolved in 150 µl 80% acetonitrile (ACN) containing 5% trifluoroacetyl (TFA) and loaded onto TiO_2 microcolumns (GL Sciences)[63]. The samples were subsequently washed with 0.1% TFA; 0.1% TFA, 80% ACN; 0.1% TFA; and 0.1% TFA, 80% ACN. The enriched products were eluted using 0.5% NH_4OH, 20% ACN; 0.5% NH_4OH, 40% ACN; and 0.5% acetic acid, 80% acetonitrile, respectively. All flow-throughs were collected and dried by speed vacuum. Samples were digested using trypsin (enzyme:protein ratio of 1:50 w/w) at 37 °C for 16 h. TFA (0.1%) was added to quench the reaction. The product was desalted using C18 stage tips. The solvent was evaporated in a speed vacuum. Peptides were dissolved in LC buffer A. Before MS analysis, peptides were separated using an UltiMate 3000 RSLCnano system (Thermo Fisher) with a C18 column (750 µm × 150 mm, 3 µm particle size) and a gradient ranging from 5% buffer B to 40% B in 105 min. The MS analysis was performed using Q-Exactive plus. The electrospray voltage was set at 2.3 kV. The ion transfer tube temperature was set at 320 °C. Auto gain control was set at 1×10^6 in the mass range from 350 to 1,800 m/z. The resolution was set at 70,000. MS/MS was triggered by the DDA module with the top 10 precursors isolated by a 2.0 m/z window. Higher-energy collisional dissociation was used to fragment peptides with normalized collision energy at 27 and resolution at 17,500. Raw data were analysed using MaxQuant (v.1.6.0.1) as previously described[62]. For parallel reaction monitoring analysis, samples were re-injected into LC–MS with the same setting. The target peptide list was imported into the parallel reaction monitoring module with the retention time window at 4 min. The result was analysed using Skyline (v.3.7).

GO enrichment analysis

$\log_2$ fold change (HD5/mock or HD5/Suramin + HD5) ≥1 was applied to filter significantly regulated proteins on the basis of the phosphor-peptide intensity dataset. Sets of genes with significant upregulation and downregulation were analysed for enrichment of GO terms using the enricher function of the clusterProfiler package (v.4.8.3)[64] in R with default parameters. The enrichment results were visualized using the R packages ggplot2 (v.3.4.4)[65] and enrichplot (v.1.20.3)[66]. For Fig. 3e, 15 significant molecular function GO terms ($\log_2$FC (HD5/mock) ≥1, adjusted $P < 0.05$) with count ≥6 were selected for plotting. For Extended Data Fig. 3c, cell component GO terms ($\log_2$FC (HD5/mock) ≥1 and $\log_2$FC (HD5/Suramin + HD5) ≥1, adjusted $P < 0.05$) were sorted by adjusted P value, and the lowest 25 were chosen for plotting. Advanced heat map plots were generated using the OmicStudio tools (https://www.omicstudio.cn/tool)[67].

Human phosphokinase array

The relative phosphorylation levels of the selected target molecules involved in signal transduction pathways in HeLa cells upon HD5 treatment were analysed using the commercially available Human Phospho-Kinase Array kit (R&D Systems, ARY003B). This kit is a membrane-based sandwich immunoassay with capture antibodies to detect 43 major human kinase phosphorylation sites spotted in duplicate on nitrocellulose membranes bound to specific target proteins present in the cell lysates. After complete homogenization of the treated cells, the whole suspension was centrifuged for 5 min at 14,000 g. The supernatants were used as whole-tissue lysates and then processed according to manufacturer protocol. Phosphorylation of captured proteins was detected with biotinylated phospho-specific detection antibodies and then visualized using chemiluminescent detection reagents (NCM, P10100). The signal produced was proportional to the amount of phosphorylation in the bound analyte. The levels of phosphorylation were quantified using the ImageJ platform (Fiji).

Transcriptomic analysis of cell lines

RNA-seq data from 10 cell types were obtained from the Sequence Read Archive and the Genome Sequence Archive as listed in the resources and reagents table (Supplementary Table 1). Additional data from 8 cell lines (HeLa, Hep-G2, Jurkat, K-562, MS751, SiHa, THP-1, U-937) were generated in our laboratory. Cells were washed three times with PBS, preserved in TRIzol reagent and then sent to Novogene for RNA extraction, library construction and sequencing. Briefly, sequencing libraries were generated using NEBNext Ultra RNA Library Prep kit for Illumina (New England Biolabs) with the index-coded samples clustered according to manufacturer instructions using a cBot Cluster Generation System with the TruSeq PE Cluster Kit v3-cBot-HS (Illumina). Libraries were sequenced using an Illumina NovaSeq 6000 to produce 150-bp paired-end reads. Raw reads were cleaned using fastp (v.0.19.7)[68] with the parameters 'fastp -g -q 5 -f 10 -u 50 -n 15 -l 30'. Cleaned reads were aligned to human reference GRCh38.p13 (GCF_000001405.39) using HISAT2 (v.2.2.1)[69] with default parameters, with transcripts then assembled and expression quantified (as TPM) using StringTie (v.2.2.1)[70] with default parameters. Data were parsed to determine, for 1,415 genes known to encode GPCRs (HGNC gene group: 'G protein-coupled receptors'; https://www.genenames.org/data/genegroup/#!/group/139)[35], the average expression across all cell lines and the number of cell lines in which TPM > 1.

To verify the RNA-seq data, transcript expression levels (nTPM) summarized per gene in 14 cell lines (A-549, CACO-2, HEK293, HeLa, Hep-G2, HT-29, Jurkat, K-562, MCF-7, MS751, PC-3, SiHa, THP-1, U-937) were downloaded from '25 RNA HPA cell line gene data' in The Human Protein Atlas database v.23.0 (http://www.proteinatlas.org/about/download)[27]. To search GPCRs that activate Gs, GPCR genes were annotated by Reactome v.86 'Identifier mapping files-Lowest level pathway diagram/Subset of the pathway-ENSEMBL to pathways' (https://reactome.org/download/current/Ensembl2Reactome.txt). GPCR-Gs genes that showed high expression (RNA-seq TPM > 1 in 18 cell lines and The Human Protein Atlas nTPM > 1 in 14 cell lines) were considered as potential HD5 receptors.

Immunoprecipitation analysis of interaction between GPCR and HD5

Hela cells (10^7) were prepared and lysed with a GPCR Extraction and Stabilization Reagent (Thermo Scientific) containing a protease inhibitor cocktail (Roche) according to manufacturer instructions. The stabilized protein receptors were in the supernatant. Protein concentrations were measured with the Enhanced BCA Protein Assay kit (Beyotime). Receptor proteins (1 mg) were incubated with 0.4 mg of biotin-labelled HD5 for 12–16 h on a rotary mixer at 4 °C. The mixture was then immobilized to 50 µl streptavidin magnetic beads (MCE) for 1 h at room temperature following manufacturer instructions. The beads were washed five times with washing buffer (PBS, 0.05% Tween-20, pH 7.4) and then eluted twice with 40 µl 1× SDS–PAGE loading buffer at 95 °C for 5 min for loading onto 4–20% SDS–PAGE gels.

LC–MS/MS analysis of HD5-interacting proteins

HD5-bound proteins enriched by streptavidin magnetic beads as described above were subjected to liquid chromatography–mass spectrometry. On-bead reduction, alkylation and tryptic digestion were performed immediately following the pulldown assay[71]. Salts and buffers were removed using a C-18 membrane filled column. The desalting samples were subjected to LC–MS/MS detection. A Nano-HPLC UltiMate 3000 RSLCnano system (Thermo Fisher) coupled with a Q-Exactive plus (a high-performance hybrid quadrupole Orbitrap mass spectrometer, Thermo Fisher) was used for the proteome detection (0.1% HCOOH in water as mobile phase A and 0.1% HCOOH in acetonitrile as mobile phase B) and the data analysed with Proteome-Discover (2.5)[72] using the UniProt database[73]: uniprot-human-reviewed yes+taxonomy 9606_20230224. The presence of the P2Y11 peptide was identified via a target searching strategy as previously reported[57].

Molecular docking simulation

The structure of P2Y11 was homologously modelled from the human P2Y1 receptor retrieved from the Protein Data Bank (PDB 4XNW). The crystal structure of the HD5 dimer was also obtained from the Protein Data Bank (PDB 1ZMP). Molecular docking was performed using the Glide algorithm to predict potential binding poses between P2Y11 and the HD5 dimer or small molecular antagonists NF157 and NF340. Docking poses were then submitted to molecular dynamics simulations for conformational optimization on Amber20 (ref. 74). In detail, the chemical structures of NF157 and NF340 were created and optimized using Chem3D and the partial atomic charges calculated using the AM1-BCC method, implemented in the Antechamber module in Amber20, to obtain the molecular mechanics parameters of NF157 and NF340. The molecular mechanics parameters from ff19SB and GAFF force field were assigned to the docking pose of HD5-P2Y11, NF157-P2Y11 and NF340-P2Y11, which were then neutralized by adding sodium/chlorine counter ions and solvated in a cuboid box of transferable interatomic potential with three points model (TIP3P) water molecules with solvent layers of 12.0 Å between solute surface and box edges, via the LEaP module. In parallel with the volume of the cuboid box, specific counts of sodium/chlorine ions were added to achieve the physiological concentration (150 mM) of NaCl in the system. After steps of minimization, heat and equilibrium, a 10-ns-production MD simulation was applied to the complexes of HD5-P2Y11, NF157-P2Y11 and NF340-P2Y11, respectively. The contributions of each ligand, including HD5, NF157 and NF340, to the binding free energy were calculated using the MM/GBSA method[75].

Extensive MD simulation of HD5-P2Y11 was also conducted using Amber20. The docking pose of HD5-P2Y11 was inserted into a preequilibrated 1,2-dioleoyl-sn-glycero-3-phosphocholine (DOPC) bilayer by using the Membrane Builder module in the CHARMM-GUI programme[76]. The solvated system was constructed according to the aforementioned protocol, and was electrostatically neutralized and physiologically treated by adding reasonable counts of sodium/chlorine ions. The SHAKE algorithm was employed to constrain all covalent bonds involving hydrogen atoms. Energy minimization was performed via the pmemd.cuda module. NVT minimization, containing 5,000 steps of steepest descent minimization and 5,000 steps of conjugated gradient minimization, was applied to the system, with the protein backbone restrained by 10.0 kcal mol^{-1} Å^{-2} and backbone Cα atoms restrained by 5 kcal mol^{-1} Å^{-2}. The system was then fully relaxed by 20,000-step steepest descent and 20,000-step conjugated gradient minimizations without any restraint to remove unfavourable contacts. Subsequently, the system was gradually heated from 0 K to 100 K in 40 ps with a time step of 0.5 fs and maintained at 100 K for 10 ps. The system was then heated from 100 K to 300 K in 160 ps with a time step of 2 fs and maintained at 300 K for 40 ps, using Langevin dynamics at a constant volume. A 200-ps density equilibration was conducted to optimize the heated system that subsequently underwent two steps of NPT ($T = 300$ K, $P = 1$ atm) equilibration with or without restraint for a total of 200 ps. Finally, the system was submitted to a 100-ns NPT ($T = 300$ K, $P = 1$ atm) production MD simulation using the pmemd.cuda module. The MD trajectory was analysed using CPPTRAJ (a C++ program in the Amber suite for analysing molecular dynamics trajectories and data) and the root-mean-square deviation was then calculated. Individual contributions of residues in HD5 and P2Y11R to the binding free energy between HD5 and P2Y11R were calculated using the MM/GBSA method through the MMPBSA.py.MPI module. Visualization of 3D structures was achieved using PyMOL and the Discovery Studio visualizer tool, and the digital data presented using GraphPad Prism 9.5.1.

Genetic knockout of *P2Y11*, β1 integrin and *CD44*, and immunoblotting assay

P2Y11 knockout stable cell lines were established using the clustered regularly interspaced short palindromic repeats/CRISPR-associated protein 9 (CRISPR/Cas9) method of gene editing[77]. Guide RNA sequences targeting *P2Y11* exon 2 were designed using CRISPR (http://tools.genome-engineering.org) and synthesized commercially (Tsingke). Single guide RNA was cloned into the peSpCas9-Puro plasmid (MiaolingBio) and the plasmid amplified by transformation into competent DH5α cells (TIANGEN). Plasmid DNA was isolated from cultures using a TIANprep Mini Plasmid kit according to manufacturer instructions. Purified plasmids were then sequenced to validate the insertion of guide RNAs into the vector using the U6 forward primer. Validated plasmids were transfected into HeLa cells using the Polyethylenimine Linear MW40000 reagent (Yeasen) as instructed by the manufacturer. On the second day post transfection, 3 μg ml^{-1} puromycin was added to the cells and the cells incubated for a total of 96 h. Cells were dissociated and diluted to 1 cell per 100 μl, and then seeded into wells of 96-well culture plates. Plates were incubated at 37 °C and 5% CO_2 in a humidified incubator for ~2 weeks and clone formation was confirmed by visual inspection. Cells were subsequently expanded into 24-well plates and when the cell density of the colonies was ~2 × 10^5, cells were collected for immunoblotting and exome sequencing.

The CRISPR/Cas9-based β1 integrin-KO or *CD44*-KO HeLa cells were established as instructed by the manufacturer (Santa Cruz Biotechnology). Briefly, to generate β1 integrin-KO cells, the integrin β1 CRISPR/Cas9 KO plasmid (h) (sc-400097) and integrin β1 HDR plasmid (h) (sc-400097-HDR) were co-transfected into HeLa cells using UltraCruz Transfection reagent (sc-395739) according to manufacturer instruction. For *CD44*-KO HeLa cells, the HCAM CRISPR/Cas9 KO plasmid (h2) (sc-400209-KO-2) and HCAM HDR Plasmid (h2) (sc-400209-HDR-2) were used to transfect HeLa cells. The medium was changed 24 h after transfection and puromycin was added into the cell culture after 72 h at the concentration of 2 μg ml^{-1}. Following ~10 days culture in puromycin-containing medium (medium was changed every other day), the puromycin-resistant cells were enriched and collected. The KO cells were defined by immunoblotting analysis.

Lysate preparation of parental and KO HeLa cells and determination of lysate protein concentration were performed as previously described. Immunoblotting samples were prepared in SDS–PAGE loading buffer supplemented with Tris(2-carboxyethyl)phosphine (NCM Biotech), heated for 10 min at 95 °C and electrophoresed using 4–20% polyacrylamide gels for 40 min at 160 V. Proteins were transferred onto PVDF membranes followed by 60 min blocking in TBS-T (10 mM Tris pH 7.4, 150 mM NaCl, 0.1% Tween-20) supplemented with 5% skimmed milk. Membranes were probed overnight on a roller band at 4 °C with anti-β1 integrin antibody (Cell Signaling Technology (CST), 4706; dilution 1:1,000), anti-CD44 antibody (CST, 3570; dilution 1:1,000) or anti-P2Y11 antibody (APR-015, Alomone; dilution 1:500). Membranes were then washed three times for 10 min with TBS-T and probed with goat anti-rabbit-HRP (dilution 1:5,000) or goat anti-mouse-AF800 (dilution 1:5,000) antibodies in TBS-T/5% skim milk for 1 h at room temperature. After two washes with TBS-T and one wash with TBS, blots were subsequently developed with chemiluminescent substrate and imaged for chemiluminescence on a ChemiDoc XRS+ System (Bio-Rad). In all cases, β-actin (66009-1-Ig; dilution 1:1,000) or GAPDH (60004-1-Ig, Proteintech; dilution 1:5,000) was used as a loading control. Band intensities were quantified using ImageJ software.

P2Y11 knock-in with the Sleeping Beauty transposon system

P2Y11 expression was rescued from the KO cells by *P2Y11* knock-in (*P2Y11* KO + KI) using the Sleeping Beauty transposon system containing the Sleeping Beauty transposon system vector and helper plasmids (gift from Yongzheng Wu). *Homo sapiens* purinergic receptor *P2Y11* gene sequence (UCSC: ENST00000321826.5) was synthesized by Tianjin Zhonghe Gene Technology on the basis of data from the UCSC Genome Browser, featuring a coding sequence fragment flanked by both the initiation codon ATG and the termination codon TAG. The vector pSBbi-GP and the target gene *P2Y11* were amplified via PCR using primers with terminal overlapping sequences of ~20–40 bp, which were recombined by mixing the vector and the target gene fragments (molecular ratio 1:3) in a recombinant enzyme system (TIANGEN, EasyGeno Rapid Recombinant Cloning kit). The recombinant plasmids were amplified and subjected to sequence identification. Validated plasmids were transfected into HeLa *P2Y11* knockout cells using Polyethylenimine Linear MW40000 reagent (Yeasen) and screened using 3 μg ml^{-1} puromycin as described above.

Immunofluorescence of cell lines

Cells were plated onto glass coverslips and adhesion assays were performed as described using Sf301 harbouring the GFP-expressing plasmid. Cells were fixed in 4% paraformaldehyde/PBS at room temperature for 15 min, followed by permeabilization with 0.1% Triton/PBS for 5 min, washing in PBS and blocking with 5% BSA/PBS for 30 min at room temperature. The coverslips were incubated with antibodies at 4 °C overnight, followed by PBS washing and incubation with fluorescein-labelled secondary antibodies as indicated, for 1 h. The coverslips were then washed and further stained with Alexa Fluor 647 or TRITC-conjugated phalloidin (Yeasen) for 30 min and mounted with DAPI-containing Fluoromount-GTM reagent (Yeasen) onto glass slides and imaged as described below.

Immunofluorescence of human colonic tissues and the corneal epithelia of guinea pigs

Human colonic tissues were embedded in OCT compound and cut into 5-μm-thick sections. The separated guinea pig corneal conjunctival tissues were rinsed with PBS three times. A small incision was made at the corneal margin, and the tissues were fixed with 0.75% paraformaldehyde for 24 h and then gradient dehydrated with 10% (1 h), 20% (overnight) and 30% (overnight) sucrose followed by embedding in OCT and cutting into 10-μm-thick sections. The OCT sections were fixed in 4% paraformaldehyde in PBS for 20 min at r.t., followed by permeabilization with 0.3% Triton X-100 in PBS for 10 min at r.t., blocking in 5% BSA in PBS for 1 h and incubation with primary antibodies against P2Y11 (APR-015, 1:200) for 12 h at 4 °C. After washing with PBS-T, sections were incubated with AF488-labelled goat anti-rabbit (EF0008, 1:500) secondary antibodies for 1 h at r.t. After counterstaining with DAPI, sections were imaged as described below.

Confocal imaging and image analysis

Fixed cells were imaged using commercialized High Intelligent and Sensitive SIM (HIS-SIM) provided by Guangzhou CSR Biotech. Images were acquired using a ×100/1.5 NA oil immersion objective (Olympus). SIM images were collected and analysed as instructed by the manufacturer[78]. Sparse deconvolution was carried out to further improve image quality[79]. For 3D reconstruction, *Z*-stack images were generated with 1–2 μm sections using an LSM 700 confocal laser scanning microscope (Zeiss) with ×40 water immersion objective with standard settings, and processed with Zen blue software and ImageJ.

MATLAB (R2023a) was used to analyse the time-sequential acquisition of real-time *Shigella* capture by filopodia extensions induced by HD5 in SiR-actin-labelled HeLa in Fig. 1. The selected images were merged into one image using the *Z*-projection tool in ImageJ Fiji. Then, the sparse deconvolution algorithm developed in MATLAB was used to eliminate readout noise and enhance the contrast of low-signal-to-noise-ratio images. The specific parameter settings of the sparse deconvolution algorithm were as follows: fixed parameters: the pixel size of the final image was 94 nm; the emission wavelength of the fluorescence probe was 647 nm; the effective numerical aperture was 2.5; we chose 3D imaging and GPU acceleration. Image property parameters: select no upsampling in a non-fluorescent background. Algorithm parameters: *t* (*z*) axis continuity used to adjust the continuity parameter along the input dataset *t* or *z* axis, set this parameter to 0.1 to avoid causing motion artefacts, sparse iterations of 50, and then selected Richardson–Lucy algorithm for iterative deconvolution. Content perception parameters: image fidelity was 150, representing the distance between the images before and after sparse reconstruction; sparsity was 2, indicating the relative sparsity constraint on reconstruction execution; the iterative deconvolution time was 50. The exact process was applied to the pictures of the bacteria corresponding to the spatial location. The cell and bacterial images were then merged and converted into fluorescent images using the Merge Channel tool in ImageJ Fiji. The numbers of bacteria that entered the cell via the grabbing and sliding patterns were counted manually.

HIFE quantification using FiloQuant

FiloQuant, an open-access software developed to specifically quantify the length, density and dynamics of filopodia and filopodia-like structures, was installed in the ImageJ platform (Fiji)[80,81]. Quantification of filopodia and filopodia-like protrusions from 10 randomly-selected single images from each group was performed using FiloQuant following manufacturer instructions[15]. Lamellipodia were measured using ImageJ as previously described[15,16]. Filopodial protrusions from live-cell imaging experiments were quantified manually.

Scanning electron microscopy

For SEM, adhesion assays were performed in the presence of 2 μM HD5 (MOI 50:1) as previously described. Cells were fixed in 4% paraformaldehyde (15 min at r.t.) and 2.5% glutaraldehyde (4 °C overnight) after PBS washing. The cells were dehydrated in graded ethanol, critical point dried with CO_2 and coated with gold-palladium beads with a diameter of 15 nm. Samples were photographed using a Zeiss scanning electron microscope at 10 kV.

Statistics and reproducibility

Statistical analyses are described in figure legends. All data were collected from at least three independent experiments in biological triplicates or more repeats, unless otherwise indicated. Data were combined and represented as mean ± s.e.m. or mean ± s.d. Results were analysed with various statistical tests using GraphPad Prism v.9.5.1 (www.graphpad.com) with $P < 0.05$ considered statistically significant. Significance levels are as follows: $^{*}P < 0.05$, $^{**}P < 0.01$, $^{***}P < 0.001$ and $^{****}P < 0.0001$; NS, not significant. Data distribution was assumed to be normal, but this was not formally tested. No statistical methods were used to predetermine sample sizes, but our sample sizes are similar to those reported in previous publications[5,6]. Advanced heat map plots (Extended Data Figs. 3b and 5a, hclust parameter: complete, Euclidean distances) were generated using OmicStudio tools (https://www.omicstudio.cn). Microscopy images are representative of at least three independent experiments. Data collection was not performed blind to the conditions of the experiments, but analysis was blinded. No animals or data points were excluded from the analysis.

Reporting summary

Further information on research design is available in the Nature Portfolio Reporting Summary linked to this article.

Data availability

The data supporting the findings of this study are available within the Article and its supplementary files. Publicly available datasets can be accessed at: HGNC (https://www.genenames.org/), Reactome v.86 (https://reactome.org/), The Human Protein Atlas 23.0 (https://www.proteinatlas.org/), Protein Data Bank (https://www.rcsb.org/), UCSC Genome Browser (https://genome.ucsc.edu/), Sequence Read Archive (SRA) (https://www.ncbi.nlm.nih.gov/sra), Genome Sequence Archive (GSA) (https://ngdc.cncb.ac.cn/gsa/). RNA-seq data generated in this study have been deposited at the Genome Sequence Archive (https://ngdc.cncb.ac.cn/search/specific?db=hra&q=HRA006201)[82,83]. Mass spectrometry proteomics data have been deposited with the ProteomeXchange Consortium via the PRIDE partner repository, with dataset identifiers PXD057832 and PXD057885. Data for the analysis are available on GitHub[84] and Zenodo[85]. All bacterial strains, original microscopy images and more relevant data are available from the corresponding author (K.Y., kaiye@xjtu.edu.cn) on reasonable request. Material transfer agreements may be required to distribute resources and materials generated in this study. Source data are provided with this paper.

Code availability

All code used to generate the data in this study is available on GitHub[84] and Zenodo[85].

References

1. Zasloff, M. Antimicrobial peptides of multicellular organisms. *Nature* **415**, 389–395 (2002).
2. Ganz, T. Defensins: antimicrobial peptides of innate immunity. *Nat. Rev. Immunol.* **3**, 710–720 (2003).
3. Ouellette, A. J. Paneth cell α-defensins in enteric innate immunity. *Cell. Mol. Life Sci.* **68**, 2215–2229 (2011).
4. Bevins, C. L. Innate immune functions of α-defensins in the small intestine. *Dig. Dis.* **31**, 299–304 (2013).
5. Xu, D. et al. Human enteric α-defensin 5 promotes *Shigella* infection by enhancing bacterial adhesion and invasion. *Immunity* **48**, 1233–1244.e6 (2018).
6. Xu, D. et al. Human enteric defensin 5 promotes *Shigella* infection of macrophages. *Infect. Immun.* **88**, e00769-19 (2019).
7. Klotman, M. E. et al. *Neisseria gonorrhoeae*-induced human defensins 5 and 6 increase HIV infectivity: role in enhanced transmission. *J. Immunol.* **180**, 6176–6185 (2008).
8. Rapista, A. et al. Human defensins 5 and 6 enhance HIV-1 infectivity through promoting HIV attachment. *Retrovirology* **8**, 45 (2011).
9. Valere, K., Lu, W. & Chang, T. L. Key determinants of human α-defensin 5 and 6 for enhancement of HIV infectivity. *Viruses* **9**, 244 (2017).
10. Valere, K., Rapista, A., Eugenin, E., Lu, W. & Chang, T. L. Human alpha-defensin HNP1 increases HIV traversal of the epithelial barrier: a potential role in STI-mediated enhancement of HIV transmission. *Viral Immunol.* **28**, 609–615 (2015).
11. Lehmann, M. J., Sherer, N. M., Marks, C. B., Pypaert, M. & Mothes, W. Actin- and myosin-driven movement of viruses along filopodia precedes their entry into cells. *J. Cell Biol.* **170**, 317–325 (2005).
12. Mattila, P. K. & Lappalainen, P. Filopodia: molecular architecture and cellular functions. *Nat. Rev. Mol. Cell Biol.* **9**, 446–454 (2008).
13. Leite, F. & Way, M. The role of signalling and the cytoskeleton during Vaccinia Virus egress. *Virus Res.* **209**, 87–99 (2015).
14. McCormick, B. A. *Shigella* gets captured to gain entry. *Cell Host Microbe* **9**, 449–450 (2011).
15. Schnupf, P. & Sansonetti, P. J. *Shigella* pathogenesis: new insights through advanced methodologies. *Microbiol. Spectr.* https://doi.org/10.1128/microbiolspec.bai-0023-2019 (2019).
16. Romero, S. et al. ATP-mediated Erk1/2 activation stimulates bacterial capture by filopodia, which precedes *Shigella* invasion of epithelial cells. *Cell Host Microbe* **9**, 508–519 (2011).
17. Sunkavalli, U. et al. Analysis of host microRNA function uncovers a role for miR-29b-2-5p in *Shigella* capture by filopodia. *PLoS Pathog.* **13**, e1006327 (2017).
18. Lanata, C. F. & Black, R. E. Estimating the true burden of an enteric pathogen: enterotoxigenic *Escherichia coli* and *Shigella* spp. *Lancet Infect. Dis.* **18**, 1165–1166 (2018).
19. Kotloff, K. L. *Shigella* infection in children and adults: a formidable foe. *Lancet Glob. Health* **5**, e1166–e1167 (2017).
20. Jacquemet, G. et al. FiloQuant reveals increased filopodia density during breast cancer progression. *J. Cell Biol.* **216**, 3387–3403 (2017).
21. Barry, D. J., Durkin, C. H., Abella, J. V. G. & Way, M. Open source software for quantification of cell migration, protrusions, and fluorescence intensities. *J. Cell Biol.* **209**, 163–180 (2015).
22. Pinaud, L. et al. Injection of T3SS effectors not resulting in invasion is the main targeting mechanism of *Shigella* toward human lymphocytes. *Proc. Natl Acad. Sci. USA* **114**, 9954–9959 (2017).
23. Allaoui, A., Sansonetti, P. J. & Parsot, C. MxiD, an outer membrane protein necessary for the secretion of the *Shigella flexneri* Ipa invasins. *Mol. Microbiol.* **7**, 59–68 (1993).
24. Lapaquette, P. et al. *Shigella* entry unveils a calcium/calpain-dependent mechanism for inhibiting sumoylation. *eLife* **6**, e27444 (2017).

25. Lafont, F., Van Nhieu, G. T., Hanada, K., Sansonetti, P. J. & van der Goot, F. G. Initial steps of *Shigella* infection depend on the cholesterol/sphingolipid raft-mediated CD44–IpaB interaction. *EMBO J.* **21**, 4449–4457 (2002).
26. Watarai, M., Funato, S. & Sasakawa, C. Interaction of Ipa proteins of *Shigella flexneri* with alpha5beta1 integrin promotes entry of the bacteria into mammalian cells. *J. Exp. Med.* **183**, 991–999 (1996).
27. Skoudy, A. et al. CD44 binds to the *Shigella* IpaB protein and participates in bacterial invasion of epithelial cells. *Cell Microbiol.* **2**, 19–33 (2000).
28. Yang, D. et al. Beta-defensins: linking innate and adaptive immunity through dendritic and T cell CCR6. *Science* **286**, 525–528 (1999).
29. Yang, D., Chen, Q., Chertov, O. & Oppenheim, J. J. Human neutrophil defensins selectively chemoattract naive T and immature dendritic cells. *J. Leukoc. Biol.* **68**, 9–14 (2000).
30. Röhrl, J., Yang, D., Oppenheim, J. J. & Hehlgans, T. Human beta-defensin 2 and 3 and their mouse orthologs induce chemotaxis through interaction with CCR2. *J. Immunol.* **184**, 6688–6694 (2010).
31. Dong, X. et al. Keratinocyte-derived defensins activate neutrophil-specific receptors Mrgpra2a/b to prevent skin dysbiosis and bacterial infection. *Immunity* **55**, 1645–1662.e7 (2022).
32. Karlsson, M. et al. A single-cell type transcriptomics map of human tissues. *Sci. Adv.* **7**, eabh2169 (2021).
33. Bouhaddou, M. et al. The global phosphorylation landscape of SARS-CoV-2 infection. *Cell* **182**, 685–712.e19 (2020).
34. Hohenegger, M. et al. $G_{s\alpha}$-selective G protein antagonists. *Proc. Natl Acad. Sci. USA* **95**, 346–351 (1998).
35. Seal, R. L. et al. Genenames.org: the HGNC resources in 2023. *Nucleic Acids Res.* **51**, D1003–D1009 (2023).
36. Gillespie, M. et al. The reactome pathway knowledgebase 2022. *Nucleic Acids Res.* **50**, D687–D692 (2022).
37. Meis, S. et al. NF546 [4,4'-(carbonylbis(imino-3,1-phenylene-carbonylimino-3,1-(4-methyl-phenylene)-carbonylimino)) -bis(1,3-xylene-alpha,alpha'-diphosphonic acid) tetrasodium salt] is a non-nucleotide P2Y11 agonist and stimulates release of interleukin-8 from human monocyte-derived dendritic cells. *J. Pharmacol. Exp. Ther.* **332**, 238–247 (2010).
38. Dreisig, K. & Kornum, B. R. A critical look at the function of the P2Y11 receptor. *Purinergic Signal.* **12**, 427–437 (2016).
39. Ng, P. Y. et al. Inhibition of cytokine-mediated JNK signalling by purinergic P2Y11 receptors, a novel protective mechanism in endothelial cells. *Cell. Signal.* **51**, 59–71 (2018).
40. Wu, Y., Ge, L., Li, S. & Song, Z. Antagonism of P2Y11 receptor (P2Y11R) protects epidermal stem cells against UV-B irradiation. *Am. J. Transl. Res.* **11**, 4738–4745 (2019).
41. Rajabi, M. et al. Functional determinants of human enteric α-defensin HD5: crucial role for hydrophobicity at dimer interface. *J. Biol. Chem.* **287**, 21615–21627 (2012).
42. Campbell-Valois, F. X. et al. A fluorescent reporter reveals on/off regulation of the *Shigella* type III secretion apparatus during entry and cell-to-cell spread. *Cell Host Microbe* **15**, 177–189 (2014).
43. Grassart, A. et al. Bioengineered human organ-on-chip reveals intestinal microenvironment and mechanical forces impacting *Shigella* infection. *Cell Host Microbe* **26**, 435–444.e4 (2019).
44. Williams, A. D. et al. Human alpha defensin 5 is a candidate biomarker to delineate inflammatory bowel disease. *PLoS ONE* **12**, e0179710 (2017).
45. Hong, J. S. et al. Application of enzyme-linked immunosorbent assay to detect antimicrobial peptides in human intestinal lumen. *J. Immunol. Methods* **525**, 113599 (2024).
46. Ghosh, D. et al. Paneth cell trypsin is the processing enzyme for human defensin-5. *Nat. Immunol.* **3**, 583–590 (2002).
47. Lehrer, R. I. & Lu, W. α-defensins in human innate immunity. *Immunol. Rev.* **245**, 84–112 (2012).
48. Chu, H. et al. Human α-defensin 6 promotes mucosal innate immunity through self-assembled peptide nanonets. *Science* **337**, 477–481 (2012).
49. Kudryashova, E. et al. Human defensins facilitate local unfolding of thermodynamically unstable regions of bacterial protein toxins. *Immunity* **41**, 709–721 (2014).
50. Fu, J. et al. Mechanisms and regulation of defensins in host defense. *Sig. Transduct. Target. Ther.* **8**, 300 (2023).
51. Vongsa, R. A., Zimmerman, N. P. & Dwinell, M. B. CCR6 regulation of the actin cytoskeleton orchestrates human beta defensin-2- and CCL20-mediated restitution of colonic epithelial cells. *J. Biol. Chem.* **284**, 10034–10045 (2009).
52. Jin, G. & Weinberg, A. Human antimicrobial peptides and cancer. *Semin. Cell Dev. Biol.* **88**, 156–162 (2019).
53. Biragyn, A. et al. Toll-like receptor 4-dependent activation of dendritic cells by beta-defensin 2. *Science* **298**, 1025–1029 (2002).
54. Kennedy, C. P2Y(11) receptors: properties, distribution and functions. *Adv. Exp. Med. Biol.* **1051**, 107–122 (2017).
55. Ledderose, C. et al. The purinergic receptor P2Y11 choreographs the polarization, mitochondrial metabolism, and migration of T lymphocytes. *Sci. Signal.* **13**, eaba3300 (2020).
56. Moreschi, I. et al. NAADP$^+$ is an agonist of the human P2Y11 purinergic receptor. *Cell Calcium* **43**, 344–355 (2008).
57. Grieshaber, N. A., Boitano, S., Ji, I., Mather, J. P. & Ji, T. H. Differentiation of granulosa cell line: follicle-stimulating hormone induces formation of lamellipodia and filopodia via the adenylyl cyclase/cyclic adenosine monophosphate signal. *Endocrinology* **141**, 3461–3470 (2000).
58. Gomez, T. M. & Robles, E. The great escape: phosphorylation of Ena/VASP by PKA promotes filopodial formation. *Neuron* **42**, 1–3 (2004).
59. Lin, Y. L., Lei, Y. T., Hong, C. J. & Hsueh, Y. P. Syndecan-2 induces filopodia and dendritic spine formation via the neurofibromin-PKA-Ena/VASP pathway. *J. Cell Biol.* **177**, 829–841 (2007).
60. Qi, A.-D., Kennedy, C., Harden, T. K. & Nicholas, R. A. Differential coupling of the human P2Y11 receptor to phospholipase C and adenylyl cyclase. *Br. J. Pharmacol.* **132**, 318–326 (2001).
61. Sato, T. et al. Single Lgr5 stem cells build crypt-villus structures in vitro without a mesenchymal niche. *Nature* **459**, 262–265 (2009).
62. King, B. F. & Townsend-Nicholson, A. Involvement of P2Y1 and P2Y11 purinoceptors in parasympathetic inhibition of colonic smooth muscle. *J. Pharmacol. Exp. Ther.* **324**, 1055–1063 (2008).
63. Kim, H. J., Li, H., Collins, J. J. & Ingber, D. E. Contributions of microbiome and mechanical deformation to intestinal bacterial overgrowth and inflammation in a human gut-on-a-chip. *Proc. Natl Acad. Sci. USA* **113**, E7–E15 (2016).
64. Yu, G., Wang, L. G., Han, Y. & He, Q. Y. clusterProfiler: an R package for comparing biological themes among gene clusters. *Omics* **16**, 284–287 (2012).
65. Villanueva, R. A. M. & Chen, Z. J. ggplot2: elegant graphics for data analysis (2nd ed.). *Measurement* **17**, 160–167 (2019).
66. Yu, G. enrichplot: visualization of functional enrichment result. Version 1.23.1. *GitHub* https://github.com/YuLab-SMU/enrichplot (2023).
67. Lyu, F. et al. OmicStudio: a composable bioinformatics cloud platform with real-time feedback that can generate high-quality graphs for publication. *Imeta* **2**, e85 (2023).

68. Chen, S., Zhou, Y., Chen, Y. & Gu, J. fastp: an ultra-fast all-in-one FASTQ preprocessor. *Bioinformatics* **34**, i884–i890 (2018).
69. Kim, D., Langmead, B. & Salzberg, S. L. HISAT: a fast spliced aligner with low memory requirements. *Nat. Methods* **12**, 357–360 (2015).
70. Pertea, M. et al. StringTie enables improved reconstruction of a transcriptome from RNA-seq reads. *Nat. Biotechnol.* **33**, 290–295 (2015).
71. Wiśniewski, J. R., Zougman, A., Nagaraj, N. & Mann, M. Universal sample preparation method for proteome analysis. *Nat. Methods* **6**, 359–362 (2009).
72. Orsburn, B. C. Proteome Discoverer—a community enhanced data processing suite for protein informatics. *Proteomes* **9**, 15 (2021).
73. Coudert, E. et al. Annotation of biologically relevant ligands in UniProtKB using ChEBI. *Bioinformatics* **39**, btac793 (2023).
74. Singh, U. C., Weiner, S. J. & Kollman, P. Molecular dynamics simulations of d(C-G-C-G-A) X d(T-C-G-C-G) with and without "hydrated" counterions. *Proc. Natl Acad. Sci. USA* **82**, 755–759 (1985).
75. Genheden, S. & Ryde, U. The MM/PBSA and MM/GBSA methods to estimate ligand-binding affinities. *Expert Opin. Drug Discov.* **10**, 449–461 (2015).
76. Wu, E. L. et al. CHARMM-GUI Membrane Builder toward realistic biological membrane simulations. *J. Comput. Chem.* **35**, 1997–2004 (2014).
77. Ran, F. A. et al. Genome engineering using the CRISPR-Cas9 system. *Nat. Protoc.* **8**, 2281–2308 (2013).
78. Huang, X. et al. Fast, long-term, super-resolution imaging with Hessian structured illumination microscopy. *Nat. Biotechnol.* **36**, 451–459 (2018).
79. Wang, C., Dang, T., Baste, J., Anil Joshi, A. & Bhushan, A. A novel standalone microfluidic device for local control of oxygen tension for intestinal-bacteria interactions. *FASEB J.* **35**, e21291 (2021).
80. Schindelin, J. et al. Fiji: an open-source platform for biological-image analysis. *Nat. Methods* **9**, 676–682 (2012).
81. Schneider, C. A., Rasband, W. S. & Eliceiri, K. W. NIH Image to ImageJ: 25 years of image analysis. *Nat. Methods* **9**, 671–675 (2012).
82. Chen, T. et al. The Genome Sequence Archive Family: toward explosive data growth and diverse data types. *Genomics Proteomics Bioinformatics* **19**, 578–583 (2021).
83. CNCB-NGDC Members and Partners. Database resources of the National Genomics Data Center, China National Center for Bioinformation in 2024. *Nucleic Acids Res.* **52**, D18–D32 (2024).
84. Xu, D. et al. *Shigella* infection is facilitated by interaction of human enteric α-defensin 5 with colonic epithelial receptor P2Y11. *GitHub* https://github.com/MengyaoGuo-xjtu/Analysis-of-HD5-interacting-proteins (2024).
85. Xu, D. et al. *Shigella* infection is facilitated by interaction of human enteric α-defensin 5 with colonic epithelial receptor P2Y11. *Zenodo* https://doi.org/10.5281/zenodo.14171198 (2024).

Acknowledgements

We thank A. Jegou and L. Cao from Institute Jacques Monod of CNRS and Université Paris Cité for scientific advice and technical assistance on pyrene assay of in vitro actin polymerization; Y. Hao and Z. Ren at the Instrument Analysis Center of Xi'an Jiaotong University for technical assistance with fluorescence and electron microscopic analysis; Y. Wu from Institut Pasteur for providing the Sleeping Beauty transposon system; Guangzhou CSR Biotech Co. Ltd for cell imaging using their commercial super-resolution microscope (HIS-SIM), data acquisition, SR image reconstruction, analysis and discussion; Q. Lu and M. Xia from Shanghai Jiaotong University for suggestions on the molecular docking simulation analysis. This work was supported by National Key R&D Program of China grants 2022YFC3400300 to K.Y.; National Natural Science Foundation of China grants 32125009 to K.Y., 32070134 to D.X., 32270188 to D.X., 82030062 to W.L. and 32222022 to Y.J.; and the Fundamental Research Funds of Xi'an Jiaotong University (xtr052023012 to D.X.).

Author contributions

D.X., K.Y., P.J.S., W.L. and N.S. conceptualized the project. D.X., M.G., X.X., G.L., S.J.B., C.W. and Y.J. developed the methodology. D.X., M.G., X.X., G.L., Yaxin Liu, C.W., T.X., C.L., Q.W., Wenying Zhao, W. Zeng, Yuezhuangnan Liu, S.L., S.Z. and Wei Zhao conducted investigations. D.X., M.G., X.X., G.L. and S.Z. performed visualization. K.Y., W.L., D.X. and Y.J. acquired funding. D.X. and K.Y. administered the project. K.Y., P.J.S., W.L. and N.S. supervised the project. D.X., M.G. and S.J.B. wrote the original draft. D.X., K.Y., P.J.S., W.L. and S.J.B. reviewed and edited the manuscript.

Competing interests

The authors declare no competing interests.

Additional information

Extended data is available for this paper at https://doi.org/10.1038/s41564-024-01901-9.

Supplementary information The online version contains supplementary material available at https://doi.org/10.1038/s41564-024-01901-9.

Correspondence and requests for materials should be addressed to Wuyuan Lu, Philippe J. Sansonetti or Kai Ye.

Peer review information *Nature Microbiology* thanks Gill Diamond and the other, anonymous, reviewer(s) for their contribution to the peer review of this work. Peer reviewer reports are available.

Reprints and permissions information is available at www.nature.com/reprints.

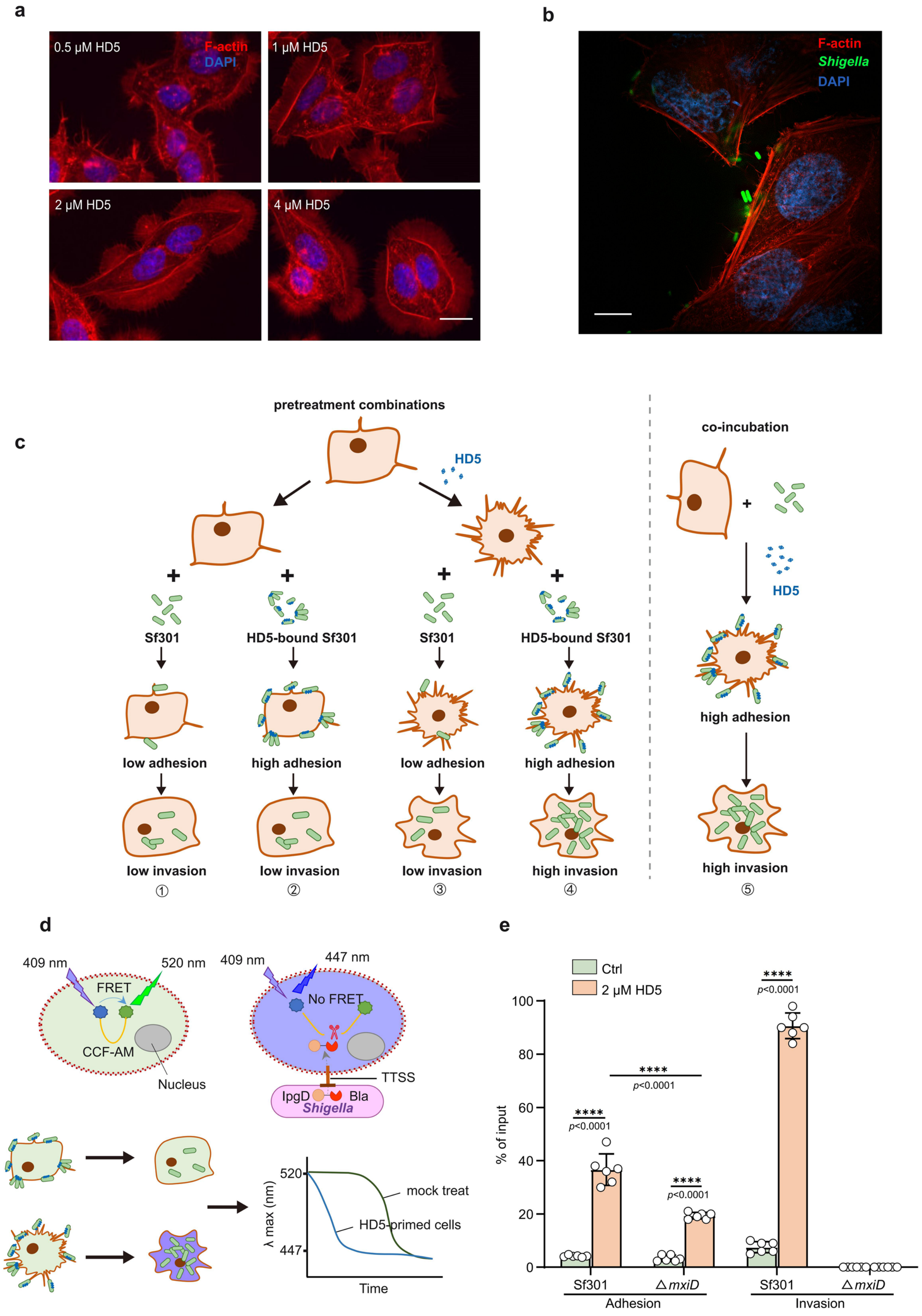

Extended Data Fig. 1 | See next page for caption.

Extended Data Fig. 1 | Influence of HD5 and *Shigella* on cytoskeleton in HeLa cells and schematic illustration of experimental procedure of *Shigella* infection and FRET assay. a, Fluorescence microscopy analysis of cytoskeleton of HeLa cells in the presence of a serial concentration of HD5. F-actin is red, and nuclei are blue (DAPI). The bars represent 20 µm. **b**, Influence of *Shigella* at MOI of 100 on the cytoskeleton of HeLa cells. F-actin is red, GFP-expressing Sf301 is green and nuclei are blue (DAPI). The bars represent 10 µm. **c**, Schematic illustration of experimental procedure of different pretreatment combinations and co-incubation. To further distinguish the effects of HD5 on bacteria and host cell respectively, HD5 was allowed to interact with *Shigella* or HeLa cells separately for 15 min, followed by 3 washes to thoroughly remove unbound defensin molecules. Different pretreatment combinations result in different levels of bacterial adhesion and invasion as shown in Fig. 2c. **d**, Illustration of Förster resonance energy transfer (FRET) assay and its application to analyze the T3SS activity of *Shigella* in its invasion in the absence of presence of HD5. **e**, Influence of 2 µM HD5 on the adhesion and invasion of *Shigella ΔmxiD* mutant in comparison with wildtype Sf301 strain. Significance compared with solvent control (0 µM) group was calculated using a one-way ANOVA (Tukey's multiple comparison Test), and indicated as the *p* value. ***$p < 0.001$ and ****$p < 0.0001$. Data are presented as mean±s.d. Results are representative of at least three independent experiments.

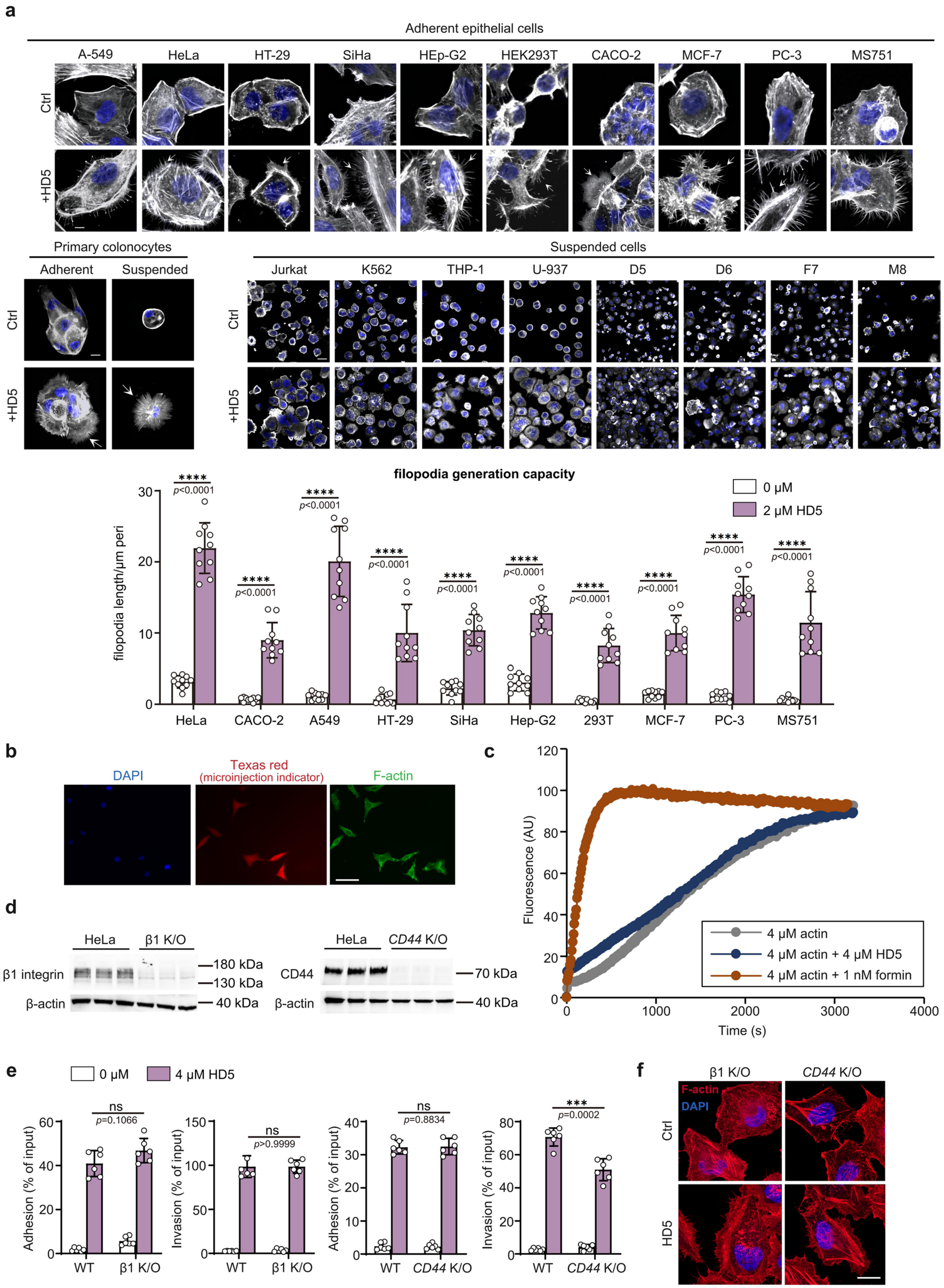

Extended Data Fig. 2 | See next page for caption.

Extended Data Fig. 2 | Influence of HD5 on cytoskeleton of different cell lines and HeLa mutants. a, Fluorescence microscopy analysis and quantification (*n* = 10) of cytoskeleton alterations in 10 adherent epithelial cell lines, primary colonocytes and 8 suspension cell lines in the absence (control) or presence of 2 μM HD5. In the upper panel, for epithelial cell lines and primary cells, the bar represents 10 μm; for suspension cells, the bar represents 20 μm. HIFE are indicated with arrows. F-actin is grey and nuclei are blue (DAPI). In the lower panel, bars indicate mean; errors, s.d. **b**, Fluorescence microscopy analysis of cytoskeleton of HeLa cells microinjected with HD5. HD5 was microinjected into HeLa cells to produce intracellular concentrations of 0.5 to 5 μM, which failed to produce any significant alteration to the cytoskeleton. Injected cells are indicated in red (with Texas Red as microinjection tracker), F-actin is green and nuclei are blue (DAPI). The bar represents 50 μm. **c**, Fluorescence absorbance analysis of *in vitro* actin polymerization dynamics of 4 μM actin in the presence of 4 μM HD5 or 1 nM formin. The addition of up to 4 μM HD5 into an *in vitro* actin polymerization system had minimal effect on the nucleation and elongation of actin filaments. Each data point represents the fluorescence value at that time point. **d**, Immunoblotting examination of β1 integrin and *CD44* knockout in HeLa cells. **e**, Influence of β1 integrin and *CD44* knockout on *Shigella* adhesion/invasion (*n* = 6). Data are presented as mean±s.d. **f**, Influence of β1 integrin and *CD44* knockout on the cytoskeleton of HeLa cells in the presence or absence of 4 μM HD5. The bar represents 20 μm. Depletion of β1 integrin subunit and *CD44* from HeLa cells by the CRISPR/Cas9 system neither affected the association of HD5 with *Shigella* adhesion and invasion, nor the formation of filopodia. Significance was determined by a two-tailed unpaired Student' s t-test, and indicated as the *p* value. ns: no signification, $^{**}p < 0.01$, $^{***}p < 0.001$ and $^{****}p < 0.0001$. All results are representative of at least three independent experiments.

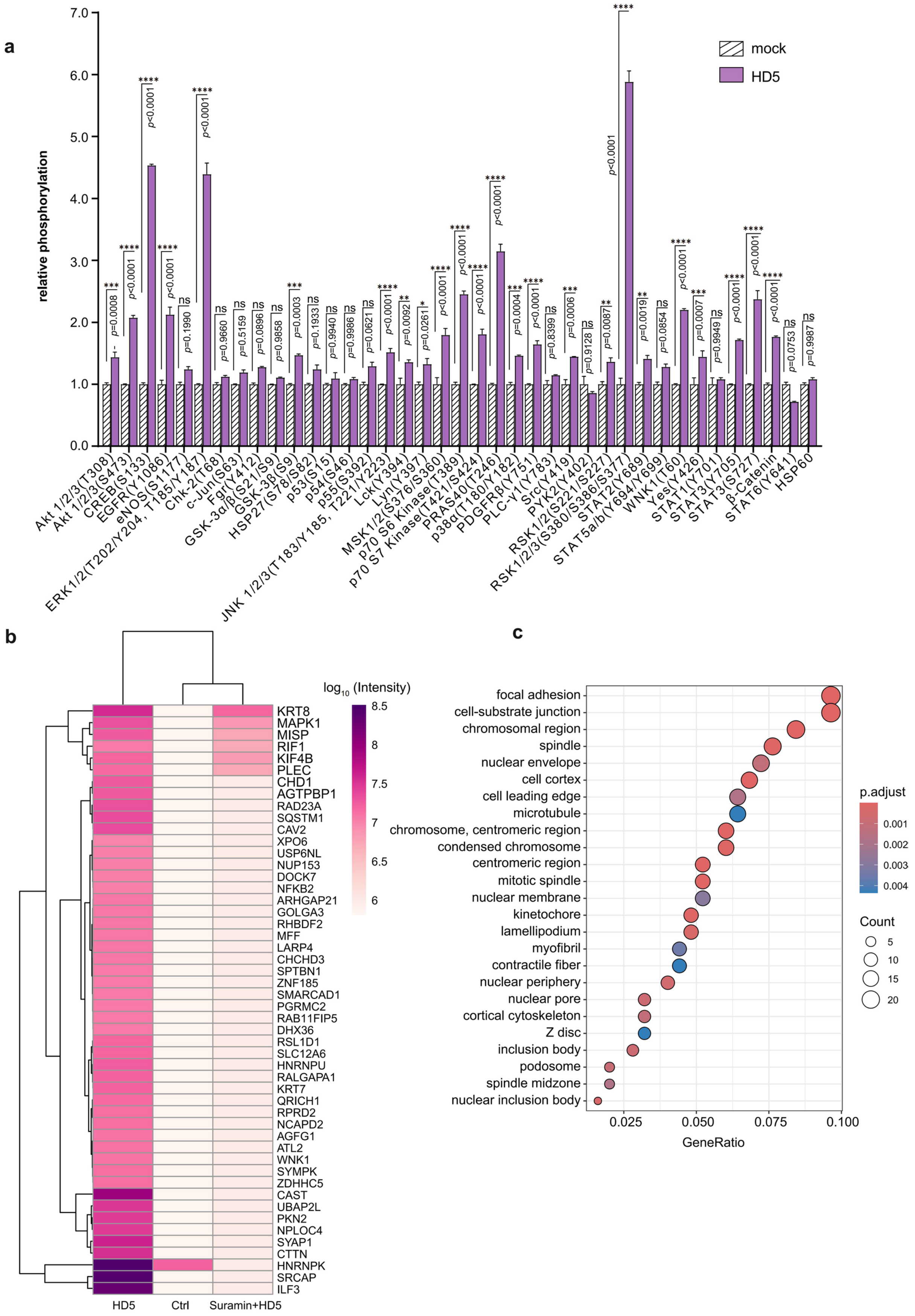

Extended Data Fig. 3 | See next page for caption.

Extended Data Fig. 3 | Human phospho-kinase antibody array analysis and phosphoproteomic analysis of HeLa cells upon HD5 treatment. a, Human phospho-kinase antibody array analysis of the phosphorylation of major kinases in the absence and presence of 4 μM HD5 as instructed by the manufacturer. Significance compared with solvent control (0 μM) group was calculated using two-tailed unpaired Student' s t-test, and indicated as the *p* value. ns: no signification, $**p < 0.01$, $***p < 0.001$ and $****p < 0.0001$. Data are presented as mean±s.d. **b**, Top 50 proteins in phosphoproteomic analysis phosphorylated upon HD5 stimulation and dephosphorylated upon suramin treatment. Many of those proteins are involved in cytoskeleton related pathway such as Ras signaling pathway (RALGAPA1), Focal adhesion (CAV2), tight junction (CTTN), PI3K-Akt signaling pathway (PKN2), intermediate-sized filaments formation (KRT8), MAPK signaling (MAPK1), determining cell morphology (MISP), Rap1 interacting factor 1(RIF1), microtubule motor activity (KIF4B),cell junction organization (PLEC) and GTPase activator activity (USP6NL). **c**, GO terms in cellular component (CC) ontology of the phosphoproteome altered by HD5. A total of 363 phosphorylated sites, including 316 pSer (pS), 30 pThr (pT), and 17pTyr (pY) were selected as high-confidence targets from phosphoproteomic analysis for subsequent gene ontology (GO) enrichment analysis. Results are representative of three independent experiments.

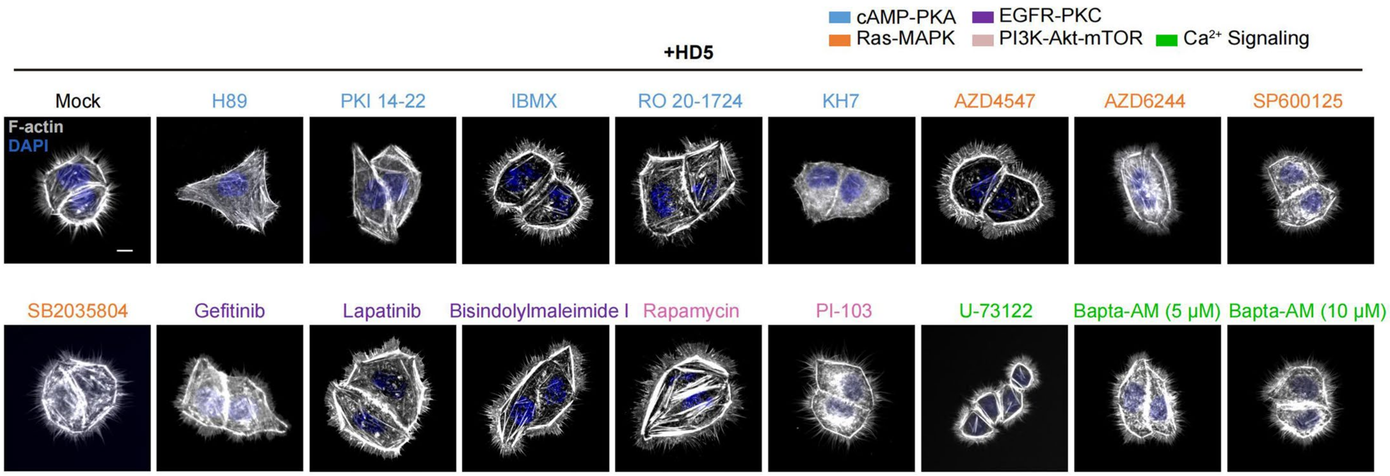

Extended Data Fig. 4 | Fluorescence microscopy analysis of influence of widely-recognized cytoskeleton-regulating pathways inhibitors on cytoskeleton of HeLa cells in the presence of 2 μM HD5. The concentrations of inhibitors used as: 20 μM H89, 20 μM PKI 14-22, 200 μM IBMX, 90 μM RO 20-1724, 50 μM KH7, 10 μM AZD4547, 2 μM AZD6244, 50 μM SP600125, 10 μM SB2035804, 10 μM Gefitinib, 10 μM Lapatinib, 1 μM Bisindolylmaleimide I, 50 μM Rapamycin, 5 μM PI-103, 2.5 μM U-73122, 5 μM Bapta-AM, 10 μM Bapta-AM. F-actin is grey, and nuclei are blue (DAPI). The bar represents 10 μm. Results are representative of three independent experiments.

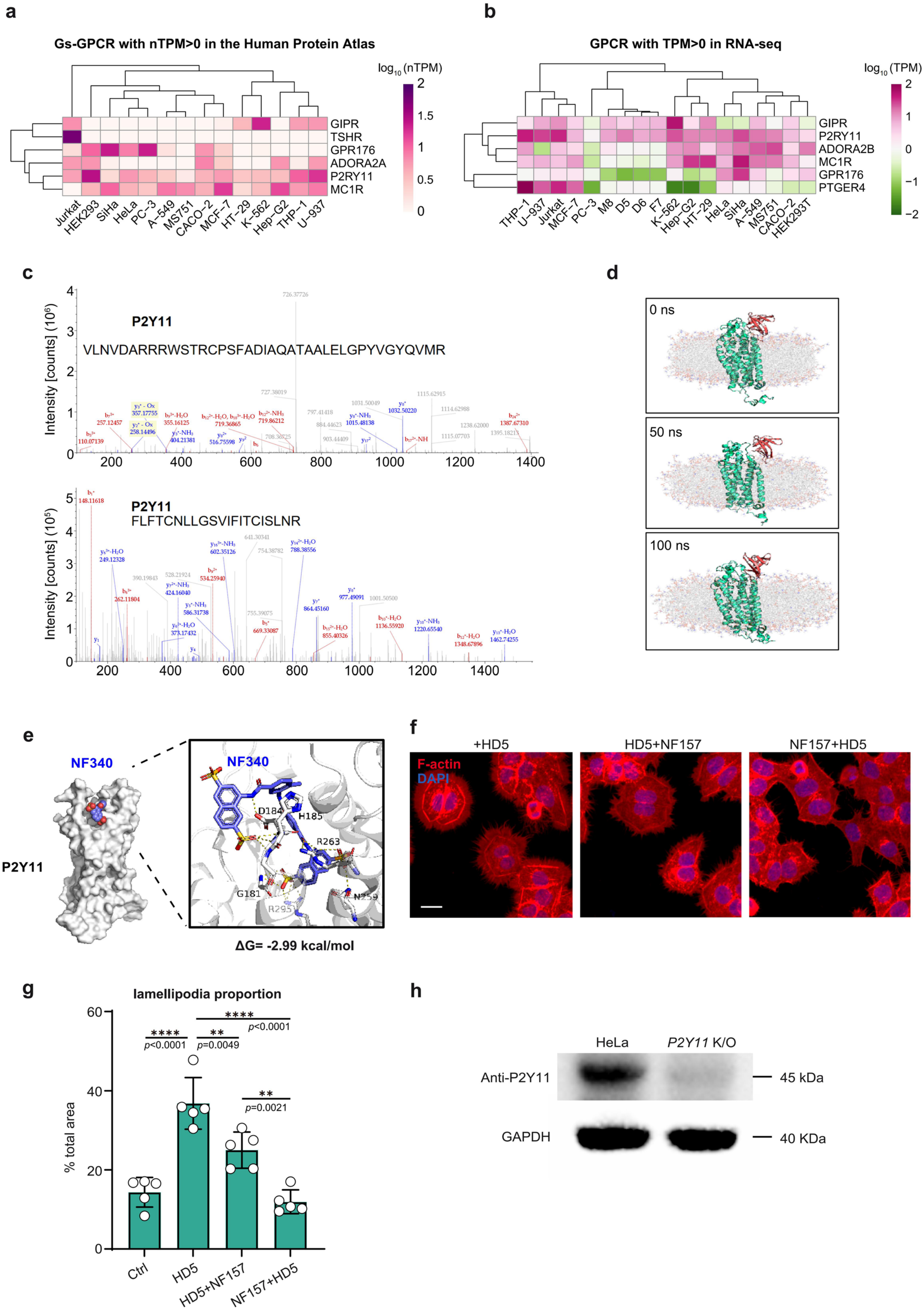

Extended Data Fig. 5 | See next page for caption.

Extended Data Fig. 5 | P2Y11 was identified as the main receptor of HD5 for HIFE generation. a, Expression analysis of Gs-coupled GPCRs in the tested cell lines using HPA database. **b**, Transcriptome analysis of the expression of GPCRs in the tested cell lines. **c**, Mass spectrometry analysis of the biotin-HD5-pulldown proteins using P2Y11-target searching strategy and two peptides of P2Y11 are present in the HD5-associated protein complex. **d**, 100-ns dynamic trajectory of simulated interaction between HD5 and P2Y11. **e**, MD simulation showing that NF340 exhibited -2.99 kcal/mol binding free energy to weakly occupy the receptor P2Y11. **f-g**, Fluorescence microscopy analysis and quantification of influence of NF157 on cytoskeleton of HeLa cells when added after HD5 addition or before HD5 addition. F-actin is red and nuclei are blue (DAPI). The bar represents 20 μm. Data are presented as mean±s.d. Significance between the indicated groups was calculated using a one-way ANOVA (Tukey' s multiple comparison Test), and p values are as follows: $^{**}p < 0.01$, $^{***}p < 0.001$ and $^{****}p < 0.0001$.**h**, Immunoblotting analysis of P2Y11 expression after CRISPR/Cas9 knockout. All results are representative of at least three independent experiments.

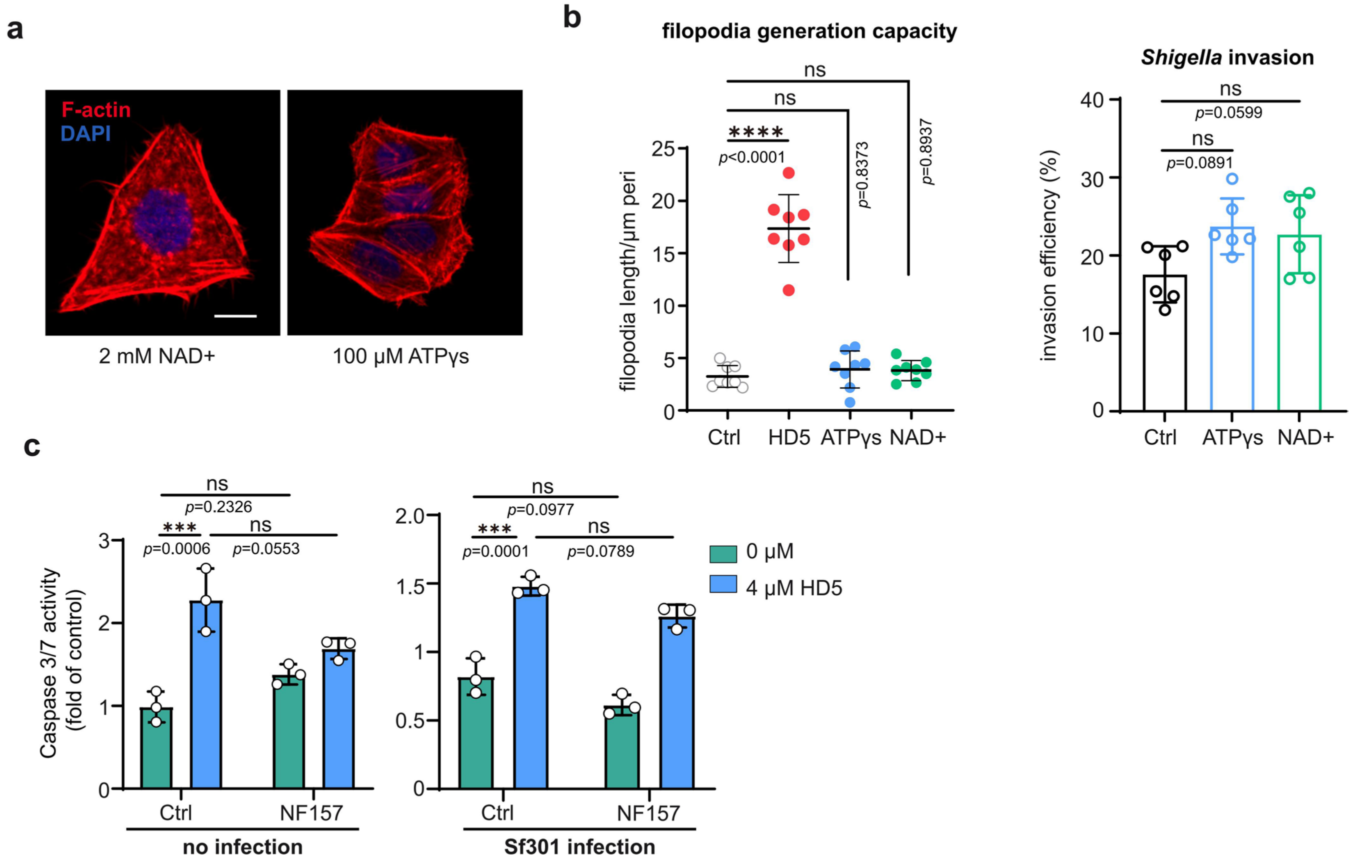

Extended Data Fig. 6 | Influence of P2Y11 agonists on HeLa cytoskeleton and the influence of HD5 on caspase activities of HeLa cells. a, b, Effects of ATPγs and NAD+ on filopodia generation capacity and bacterial invasion efficiency (*n* = 8). In **a**, F-actin is red and nuclei are blue (DAPI), the bar represents 10 μm; in **b**, Data are presented as mean±s.d. **c**, In non-infected (left panel) and infected (right panel) conditions, the caspase activities (Caspase 3/7) of HeLa cells were assessed in the presence or absence of 4 μM HD5 (*n* = 3). Significance between indicated groups was calculated using a one-way ANOVA (Dunnett's multiple comparison Test for **b** and Tukey's multiple comparison for **c**), and indicated as the *p* values. ns, not significant, $*p < 0.05$, $**p < 0.01$, $***p < 0.001$ and $****p < 0.0001$. All results are representative of at least three independent experiments.

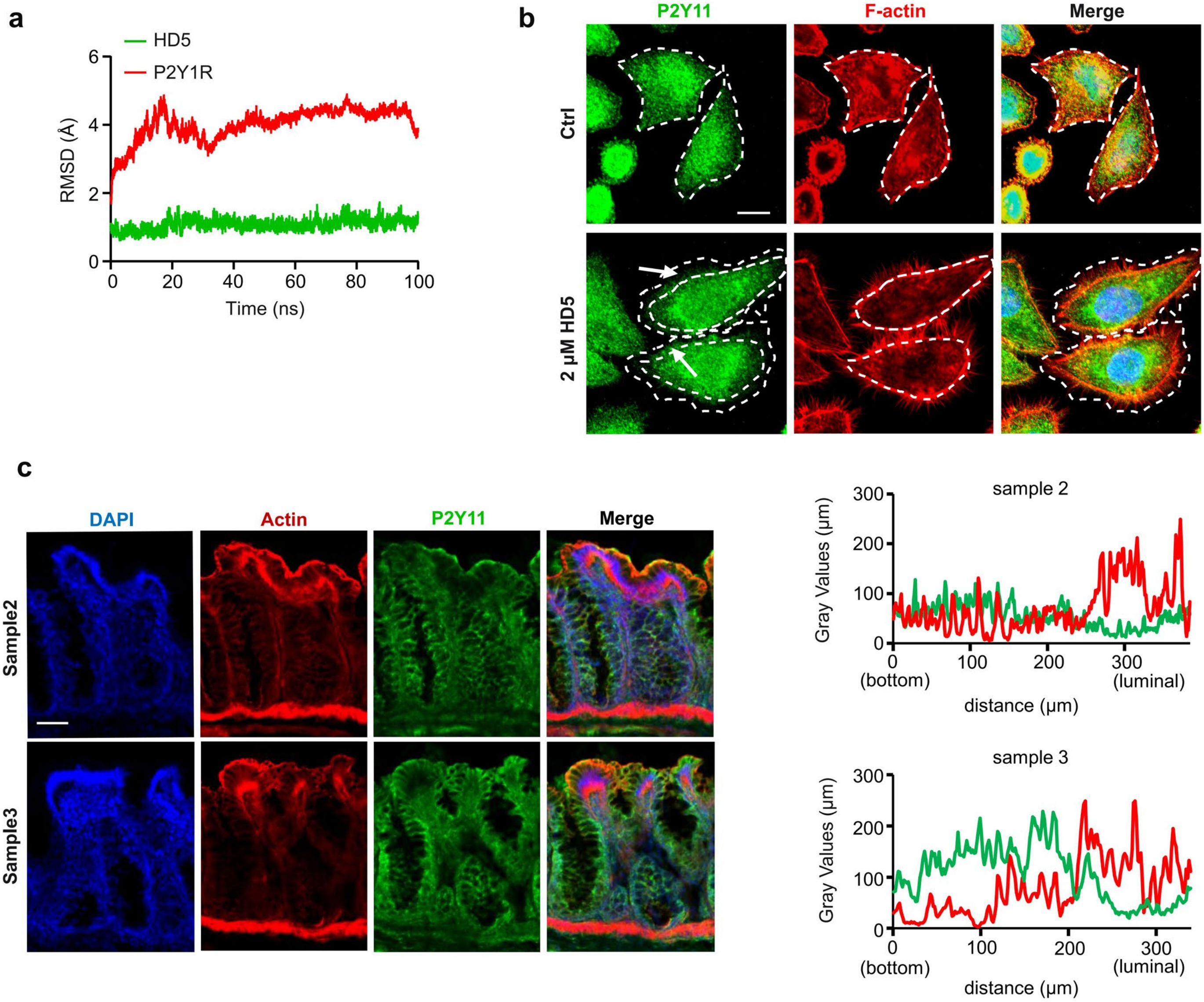

Extended Data Fig. 7 | MD analysis of HD5-P2Y11 interaction and distribution of P2Y11 in HeLa cells and human colonic samples. **a**, Root-mean-square deviation variance analysis of the steady engagement of HD5 with P2Y11 after 50 ns in the 100-ns dynamic trajectory. **b**, Fluorescence microscopy analysis of P2Y11 distribution in the absence or presence of 2 µM HD5 in HeLa cells. P2Y11 is green, F-actin is red and nuclei are blue (DAPI). Cell outlines are indicated by the dash lines and arrows. The bar represents 10 µm. **c**, Fluorescence microscopy analysis of P2Y11 distribution in two human colonic tissue (samples 2 and 3). P2Y11 is green, F-actin is red, and nuclei are blue (DAPI). The bar represents 100 µm. The right panels show gray values of P2Y11 signals in the apical and basolateral regions in human colonic crypt in the samples. All results are representative of at least three independent experiments.

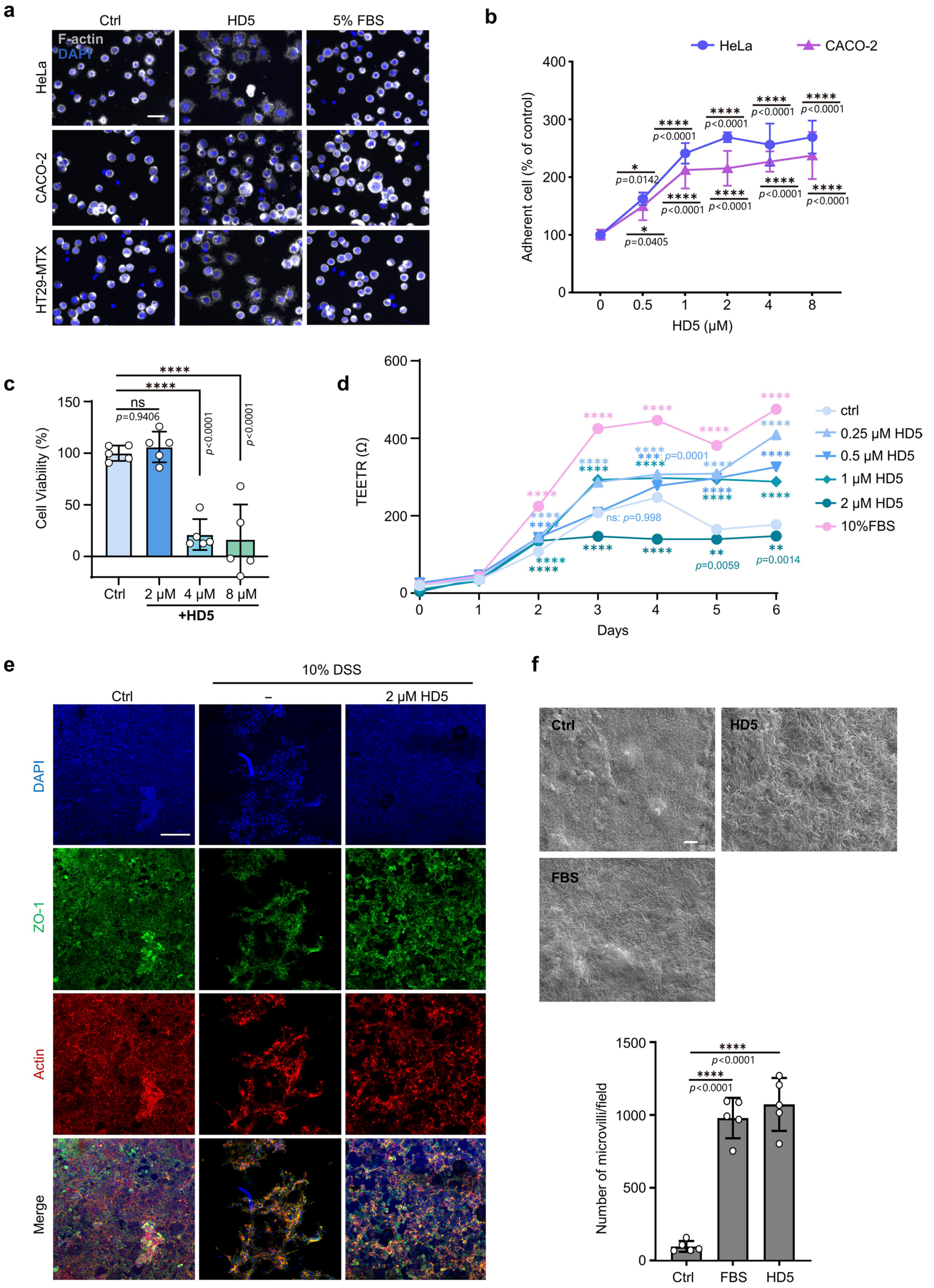

Extended Data Fig. 8 | See next page for caption.

Extended Data Fig. 8 | Influence of HD5 on cell adhesion, cell viability, TEER, DSS-damage and microvilli generation of epithelial cells. a, b, Fluorescence microscopy analysis of influence of initial adherence on HeLa, CACO-2 and HT29-MTX cells in the presence of 2 µM HD5 for 30 min (**a**) and quantification of cell attachment on petri dishes assessed by crystal violet staining 1 h post-seeding (**b**). F-actin is grey and nuclei are blue (DAPI). The bars represent 1 µm. **c**, Effects of different concentrations of HD5 on cell viability after 48-hour treatment ($n = 5$). **d**, The influence of different concentrations of HD5 on the trans-epithelial electrical resistance (TEER) during the polarization process of CACO-2 cells. **e**, Fluorescence microscopy analysis of the protective effect of HD5 on intestinal epithelial barrier upon 10% DSS damage. ZO-1 is green, F-actin is red and nuclei are blue (DAPI). The bars represent 100 µm. **f**, SEM analysis ($n = 5$) of the microvilli on polarized CACO-2 cells cultured in transwell for 5 days in the absence (control) or presence of 2 µM HD5. The bars represent 1 µm. Data are presented as mean±s.d. (**b**-**d**, **f**). Significance between indicated groups was calculated using a one-way ANOVA (Dunnett's multiple comparison Test), and indicated as the *p* value. ns, not significant, $^{*}p < 0.05$, $^{**}p < 0.01$, $^{***}p < 0.001$, $^{****}p < 0.0001$. All results are representative of at least three independent experiments.

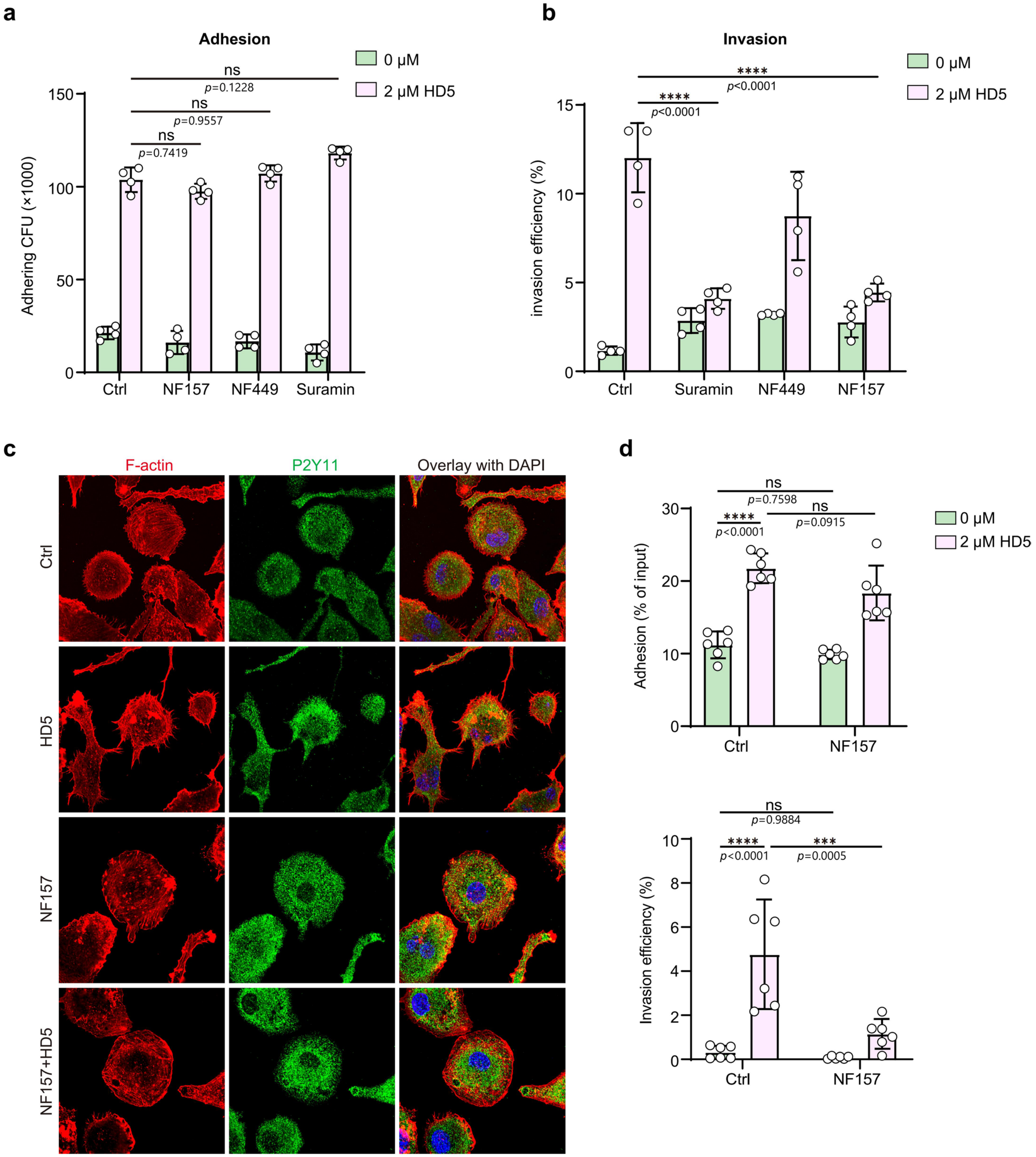

Extended Data Fig. 9 | Influence of P2Y11 antagonists on *Shigella* infection in epithelial cells and macrophage. **a**, Effect of P2Y11 antagonists (suramin, NF449 and NF157) on *Shigella* adhesion in the absence or presence of 2 μM HD5 ($n = 4$). **b**, Influence of suramin, NF449, NF157 on the invasion efficiency of Sf301 in non-polarized CACO-2 cells in the presence of 2 μM HD5 for 30 min ($n = 4$). Adhesion is defined as the total number (colony-forming unit, CFU) of CACO-2 cell-associated bacteria after 10-minute centrifuge. Invasion is expressed as the CFU of intracellular bacteria in CACO-2 cells in the next 30 min. Invasion efficiency is presented as ratio of invasion/adhesion. **c**, Fluorescence microscopy analysis examination of NF157 on cytoskeleton of PMA-differentiated THP-1 cells in the presence of 2 μM HD5. F-actin is red, P2Y11 is green and nuclei are blue (DAPI). The bar represents 10 μm. **d**, Influence of NF157 on the adhesion and invasion efficiency of *Shigella* in PMA-differentiated THP-1cells in the presence or absence of 2 μM HD5 ($n = 6$). Data are presented as mean±s.d. (**a**, b, d). Significance was determined by a one-way ANOVA (Dunnett's multiple comparison Test for **a, b** and Tukey's multiple comparison Test for **d**), and indicated as the *p* value. ns: no signification, $^{**}p < 0.01$, $^{***}p < 0.001$ and $^{****}p < 0.0001$. All results are representative of at least three independent experiments.

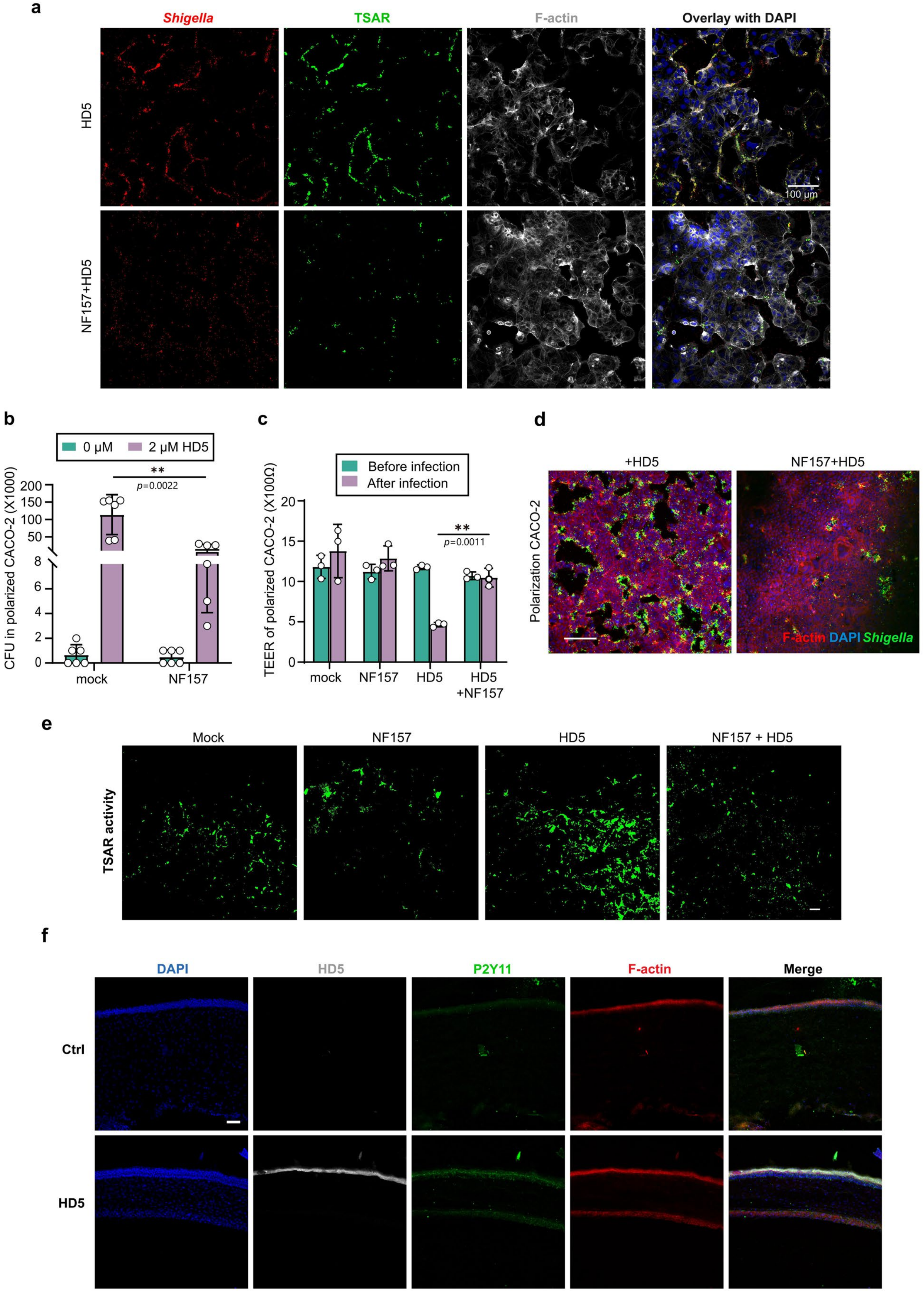

Extended Data Fig. 10 | See next page for caption.

Extended Data Fig. 10 | Influence of NF157 on Shigella infection in CACO-2 cells and P2Y11 expression in corneal epithelial cells of guinea pigs. **a**, Fluorescence microscopy analysis of influence of NF157 on the TSAR activation of Sf301 in non-polarized CACO-2 cells. F-actin is grey, *Shigella* bacteria are red, GFP-expressing bacteria are green and nuclei are stained with DAPI (blue). The bar represents 100 µm. **b**-**d**, Influence of NF157 on intracellular CFU ($n = 6$) (**b**), trans-epithelial electrical resistance ($n = 3$) (TEER, **c**) and epithelial integrity (**d**) of polarized CACO-2 cells infected with *Shigella* in the absence or presence of HD5. F-actin is red. Bacteria are green and nuclei are stained with DAPI (blue), and the bars represent 100 µm. Data are presented as mean±s.d. (b, c). Significance was determined by a two-tailed unpaired Student' s t-test (b, c), and indicated as the p value. ns: no signification, $^{**}p < 0.01$, $^{***}p < 0.001$ and $^{****}p < 0.0001$. **e**, Influence of NF157 on the *Shigella* T3SS activation (TSAR activity) on gut-on-chip with constant flow at the rate to 20 µL/h. The bars represent 50 µm. **f**. Immunofluorescence analysis of expression of P2Y11 in corneal epithelial cells of guinea pigs in the absence (upper panels) or presence (lower panels) of HD5 (Rhodamine-tagged). F-actin is red, P2Y11 is green, HD5 is grey and nuclei are stained with DAPI (blue), and the bars represent 100 µm. All results are representative of at least three independent experiments.

nature portfolio

Corresponding author(s): Kai Ye, Philippe Sansonetti, Wuyuan Lu

Last updated by author(s): Nov 15, 2024

Reporting Summary

Nature Portfolio wishes to improve the reproducibility of the work that we publish. This form provides structure for consistency and transparency in reporting. For further information on Nature Portfolio policies, see our Editorial Policies and the Editorial Policy Checklist.

Statistics

For all statistical analyses, confirm that the following items are present in the figure legend, table legend, main text, or Methods section.

n/a	Confirmed	
☐	☒	The exact sample size (*n*) for each experimental group/condition, given as a discrete number and unit of measurement
☐	☒	A statement on whether measurements were taken from distinct samples or whether the same sample was measured repeatedly
☐	☒	The statistical test(s) used AND whether they are one- or two-sided *Only common tests should be described solely by name; describe more complex techniques in the Methods section.*
☐	☒	A description of all covariates tested
☐	☒	A description of any assumptions or corrections, such as tests of normality and adjustment for multiple comparisons
☐	☒	A full description of the statistical parameters including central tendency (e.g. means) or other basic estimates (e.g. regression coefficient) AND variation (e.g. standard deviation) or associated estimates of uncertainty (e.g. confidence intervals)
☐	☒	For null hypothesis testing, the test statistic (e.g. *F*, *t*, *r*) with confidence intervals, effect sizes, degrees of freedom and *P* value noted *Give P values as exact values whenever suitable.*
☒	☐	For Bayesian analysis, information on the choice of priors and Markov chain Monte Carlo settings
☒	☐	For hierarchical and complex designs, identification of the appropriate level for tests and full reporting of outcomes
☒	☐	Estimates of effect sizes (e.g. Cohen's *d*, Pearson's *r*), indicating how they were calculated

Our web collection on statistics for biologists contains articles on many of the points above.

Software and code

Policy information about availability of computer code

Data collection	1. Western blot: ChemiDocTM XRS+ Imaging System (Bio-Rad). 2. Microscopy imaging: LSM700 (Carl Zeiss), HIS-SIM, Sigma300 FE-SEM, Leica Biosystems. 3. RNA-sequencing data: Sequencing libraries were prepared with the NEBNext® UltraTM RNA Library Prep Kit for Illumina® (NEB, USA) and clustered on a cBot Cluster Generation System using TruSeq PE Cluster Kit v3-cBot-HS (Illumia). The libraries were then sequenced on an Illumina NovaSeq 6000. 4. Proteomics data: Data collection was performed using liquid chromatography-tandem mass spectrometry (LC-MS/MS) with a Q-Exactive plus instrument.
Data analysis	Scripts for data analysis are available on GitHub and Zenodo: https://github.com/MengyaoGuo-xjtu/Analysis-of-HD5-interacting-proteins; https://doi.org/10.5281/zenodo.14171198. Specific softwares include : 1.Statistics and graphing: GraphPad Prism v9.5.1; ggplot2 v3.4.4; OmicStudio tools; R v4.4.1. 2.Proteomics analysis: clusterProfiler v4.8.3; enrichplot v1.20.3; MaxQuant v1.6.0.1; ProteomeDiscover v2.5; Skyline v3.7. 3.RNA-seq analysis: HISAT2 v2.2.1; StringTie v2.2.1. 4.Molecular docking simulation analysis: Amber20 v20; Chem3D v9.0; PyMOL v2.5.0. 5.Microscopic image analysis: Fiji v2.0.0; Filoquant v1.0.0; MATLAB v R2023a; ZEN blue Digital Imaging for Light Microscopy v2009.

For manuscripts utilizing custom algorithms or software that are central to the research but not yet described in published literature, software must be made available to editors and reviewers. We strongly encourage code deposition in a community repository (e.g. GitHub). See the Nature Portfolio guidelines for submitting code & software for further information.

Data

Policy information about availability of data

All manuscripts must include a data availability statement. This statement should provide the following information, where applicable:

- Accession codes, unique identifiers, or web links for publicly available datasets
- A description of any restrictions on data availability
- For clinical datasets or third party data, please ensure that the statement adheres to our policy

The authors declare that the data supporting the findings of this study are available within the Article and Supplementary files with source data provided. Publicly available datasets can be accessed at: HGNC (https://www.genenames.org/); Reactome v86 (https://reactome.org/); The Human Protein Atlas 23.0 (https://www.proteinatlas.org/); Protein Data Bank (https://www.rcsb.org/); UCSC Genome Browser (https://genome.ucsc.edu/); Sequence Read Archive (SRA) (https://www.ncbi.nlm.nih.gov/sra); Genome Sequence Archive (GSA) (https://ngdc.cncb.ac.cn/gsa/). RNA-seq data generated in this study have been deposited at the Genome Sequence Archive (https://ngdc.cncb.ac.cn/search/specific?db=hra&q=HRA006201). Mass spectrometry proteomics data have been deposited with the ProteomeXchange Consortium via the PRIDE partner repository, with dataset identifiers PXD057832 and PXD057885. Data for the analyses are available on GitHub and Zenodo: https://github.com/MengyaoGuo-xjtu/Analysis-of-HD5-interacting-proteins; https://doi.org/10.5281/zenodo.14171198. All bacterial strains, original microscopy images and more relevant data are available from the corresponding author upon reasonable request (Kai Ye, kaiye@ xjtu.edu.cn). Material transfer agreements may be required to distribute resources and materials generated in this study.

Research involving human participants, their data, or biological material

Policy information about studies with human participants or human data. See also policy information about sex, gender (identity/presentation), and sexual orientation and race, ethnicity and racism.

Reporting on sex and gender	This study did not consider sex and gender. A total of five patients, two males and three females, aged 2-11 months with congenital megacolon, were recruited.
Reporting on race, ethnicity, or other socially relevant groupings	The study did not consider race, ethnicity, or other relevant social groupings. All five patients were of Han ethnicity and were recruited from Shaanxi province, China.
Population characteristics	Five 2~11-month-old patients (two males and three females) of Han nationality in Shaanxi Province diagnosed with congenital megacolon.
Recruitment	The participants were recruited randomly from patients who had congenital megacolon ostomy in the Affiliated Children's Hospital of Xi'an Jiaotong University through full disclosure of the study details by clinicians and researchers. Informed consent was obtained from the guardians of all tissue donors. There are no self-selection bias or other bias.
Ethics oversight	Ethics Committee of Hospital of Stomatology of Xi'an Jiaotong University (Ethics approval No. 2024-XJKQIEC-QT-0026-001)

Note that full information on the approval of the study protocol must also be provided in the manuscript.

Field-specific reporting

Please select the one below that is the best fit for your research. If you are not sure, read the appropriate sections before making your selection.

☒ Life sciences ☐ Behavioural & social sciences ☐ Ecological, evolutionary & environmental sciences

For a reference copy of the document with all sections, see nature.com/documents/nr-reporting-summary-flat.pdf

Life sciences study design

All studies must disclose on these points even when the disclosure is negative.

Sample size	Sample size is mentioned for each experiment. No statistical methods were used to predetermine sample sizes, but our sample sizes are similar to those reported in previous publications.
Data exclusions	No data were excluded.
Replication	The experimental design incorporated a minimum of three biological replicates, outlined in figure legends and methods. Data presented in the paper are representative of at least three independent experiments to ensure data consistence.
Randomization	All aspects were randomized.
Blinding	Data collection was not performed blind to the conditions of the experiments, but analysis was blinded.

Reporting for specific materials, systems and methods

We require information from authors about some types of materials, experimental systems and methods used in many studies. Here, indicate whether each material, system or method listed is relevant to your study. If you are not sure if a list item applies to your research, read the appropriate section before selecting a response.

Materials & experimental systems

n/a	Involved in the study
☐	☒ Antibodies
☐	☒ Eukaryotic cell lines
☒	☐ Palaeontology and archaeology
☐	☒ Animals and other organisms
☒	☐ Clinical data
☒	☐ Dual use research of concern
☒	☐ Plants

Methods

n/a	Involved in the study
☒	☐ ChIP-seq
☒	☐ Flow cytometry
☒	☐ MRI-based neuroimaging

Antibodies

Antibodies used

Anti-Phospho-PKA Substrate (RRXS*/T*) (100G7E) Rabbit monoclonal antibody (Cell Signaling Technology, Cat#: 9624; CloneNo. 100G7E; Dilution 1:1000 for immunoblotting)
Anti-Human P2Y11 Receptor polyclonal antibody (Alomone Labs, Cat#: APR-015; RRID: AB_2040072; Dilution 1:500 for immunoblotting; 1:200 for immunofluorescence staining)
Anti-human CD44 (156-3C11) monoclonal antibody (Cell Signaling Technology, Cat#: 3570; CloneNo. 156-3C11; RRID: AB_2076465; Dilution 1:1000 for immunoblotting)
Anti-human integrin β1 monoclonal antibody (Cell Signaling Technology, Cat#: 4706; RRID: AB_823544; Dilution 1:1000 for immunoblotting)
Anti- GAPDH monoclonal antibody (Proteintech, Cat#: 60004-1-Ig; CloneNo. 1E6D9; RRID: AB_2107436; Dilution 1:5000 for immunoblotting)
Anti-beta actin monoclonal antibody (Proteintech, Cat#: 66009-1-Ig; CloneNo. 2D4H5; RRID: AB_2687938; dilution 1:1000 for immunoblotting)
Goat Anti-Rabbit IgG (H+L) - Alexa Fluor 488 (Sparkjade, Cat#: EF0008; RRID: AB_2892574; Dilution 1:500 for immunofluorescence staining)
HRP-conjungated Goat Anti-Mouse IgG (Abbkine, Cat#: A21010; RRID: AB_2728771; Dilution 1:5000 for immunoblotting)
HRP-conjungated Goat Anti-Rabbit IgG (Abbkine, Cat#: A21020; Dilution 1:5000 for immunoblotting)

Validation

Anti-Phospho-PKA Substrate (RRXS*/T*) (100G7E) Rabbit monoclonal antibody (Cell Signaling Technology, Cat#: 9624)
Manufacturer's website: https://www.cellsignal.com/products/primary-antibodies/phospho-pka-substrate-rrxs-t-100g7e-rabbit-mab/9624
Species specificity: All Species Expected
Applications: WB,IP

Anti-Human P2Y11 Receptor polyclonal antibody (Alomone Labs, Cat#: APR-015)
Manufacturer's website: https://www.alomone.com/p/anti-p2y11-receptor/APR-015;
Species specificity: Human
Applications: ICC, IF, IFC, IP, WB

Anti-human CD44 (156-3C11) monoclonal antibody (Cell Signaling Technology, Cat#: 3570)
Manufacturer's website: https://www.cellsignal.com/products/primary-antibodies/cd44-156-3c11-mouse-mab/3570;
Species specificity: Human
Applications: WB,IP, IHC, IF, F

Anti-human integrin β1 monoclonal antibody (Cell Signaling Technology, Cat#: 4706)
Manufacturer's website: https://www.cellsignal.com/products/primary-antibodies/integrin-b1-antibody/4706;
Species specifies: Human, Mouse, Rat, Monkey
Applications: WB

Anti- GAPDH monoclonal antibody (Proteintech, Cat#: 60004-1-Ig)
Manufacturer's website: https://www.ptglab.com/products/GAPDH-Antibody-60004-1-Ig.htm;
Species specificity: Human, Mouse, Rat, Pig, Zebrafish, Yeast, Plant
Applications: WB,IP, IHC, IF, FC

Anti-beta actin monoclonal antibody (Proteintech, Cat#: 66009-1-Ig)
Manufacturer's website: https://www.ptglab.com/Products/Pan-Actin-Antibody-66009-1-Ig.htm
Species specificity: Human, Mouse, Rat, Pig, Rabbit, Canine, Monkey, Chicken, Zebrafish, Hamster
Applications: WB,IP, IHC, IF/ICC, FC

Eukaryotic cell lines

Policy information about cell lines and Sex and Gender in Research

Cell line source(s)	A-549 (Human; lung; ATCC); CACO-2 (Human; Colon; ATCC); HCOLON (Human; Colon; This paper); HEK293T (Human; Kidney; ATCC); HeLa (Human; Cervix; ATCC); Hep-G2 (Human; LIver; ATCC); HT-29 (Human; Colon; ATCC); Jurkat (Human; Peripheral blood; ATCC); K-562 (Human; Marrow; ATCC); MCF-7 (Human; Breast; ATCC); MS751 (Human; Cervix; ATCC); PC-3 (Human; Prostate; ATCC); SiHa (Human; Cervix; ATCC); THP-1 (Human; Peripheral blood; ATCC); U-937 (Human; Pleural effusion; ATCC). LCL5 (D5) (Human; B lymphocyte; Provided by Leming Shi); LCL6 (D6) (Human; B lymphocyte; Provided by Leming Shi); LCL7 (D7) (Human; B lymphocyte; Provided by Leming Shi); LCL8 (D8) (Human; B lymphocyte; Provided by Leming Shi); The D5, D6, D7, and D8 cell lines are human immortalized B-lymphoblastoid cell lines derived from four healthy volunteers of a family quartet, as part of the Taizhou Longitudinal Study in Taizhou, Jiangsu, China. These cell lines were provided by Dr. Leming Shi and are detailed in the publication 'Quartet RNA reference materials improve the quality of transcriptomic data through ratio-based profiling,' published in Nature Biotechnology in 2023 (https://doi.org/10.1038/s41587-023-01867-9).
Authentication	The authenticity of the cell line is based on the provider's validation.
Mycoplasma contamination	The cell line was tested for mycoplasma and yielded negative results.
Commonly misidentified lines (See ICLAC register)	None of cell lines used in the paper is in ICLAC list.

Animals and other research organisms

Policy information about studies involving animals; ARRIVE guidelines recommended for reporting animal research, and Sex and Gender in Research

Laboratory animals	6~8-week-old female pathogen-free Hartley guinea pig.
Wild animals	The study did not involve wild animals.
Reporting on sex	The study used aged 6–8 weeks and weighing 120~250 g famale guinea pigs in the Sereny test.
Field-collected samples	The study did not use Field-collected samples .
Ethics oversight	The animals used in this study were acquired from the Experimental Animal Center of Xi'an Jiao tong University. The animal studies were approved by t the Biomedical Ethics Committee of Health Science Center of Xi'an Jiaotong University.

Note that full information on the approval of the study protocol must also be provided in the manuscript.

Plants

Seed stocks	N/A
Novel plant genotypes	N/A
Authentication	N/A